Measuring neutron star tidal deformability with Advanced LIGO: a Bayesian analysis of neutron star - black hole binary observations

Prayush Kumar,[1] Michael Pürrer,[2] and Harald P. Pfeiffer[1,3,2]

[1] *Canadian Institute for Theoretical Astrophysics, 60 St. George Street, University of Toronto, Toronto, ON M5S 3H8, Canada**
[2] *Albert Einstein Institute, Am Mühlenberg, Golm, Germany*
[3] *Canadian Institute for Advanced Research, 180 Dundas St. West, Toronto, ON M5G 1Z8, Canada*

(Dated: October 20, 2016)

The pioneering discovery of gravitational waves (GW) by Advanced LIGO has ushered us into an era of observational GW astrophysics. Compact binaries remain the primary target sources for GW observation, of which neutron star - black hole (NSBH) binaries form an important subset. GWs from NSBH sources carry signatures of (a) the tidal distortion of the neutron star by its companion black hole during inspiral, and (b) its potential tidal disruption near merger. In this paper, we present a Bayesian study of the measurability of neutron star tidal deformability $\Lambda_{\rm NS} \propto (R/M)^5_{\rm NS}$ using observation(s) of inspiral-merger GW signals from disruptive NSBH coalescences, taking into account the crucial effect of black hole spins. First, we find that if non-tidal templates are used to estimate source parameters for an NSBH signal, the bias introduced in the estimation of non-tidal physical parameters will only be significant for loud signals with signal-to-noise ratios greater than $\simeq 30$. For similarly loud signals, we also find that we can begin to put interesting constraints on $\Lambda_{\rm NS}$ (factor of $1-2$) with individual observations. Next, we study how a population of realistic NSBH detections will improve our measurement of neutron star tidal deformability. For an astrophysically likely population of *disruptive* NSBH coalescences, we find that $20-35$ events are sufficient to constrain $\Lambda_{\rm NS}$ within $\pm 25-50\%$, depending on the neutron star equation of state. For these calculations we assume that LIGO will detect black holes with masses within the astrophysical *mass-gap*. In case the mass-gap remains *preserved* in NSBHs detected by LIGO, we estimate that approximately 25% additional detections will furnish comparable $\Lambda_{\rm NS}$ measurement accuracy. We find these results encouraging, and recommend that an effort to measure $\Lambda_{\rm NS}$ be planned for upcoming NSBH observations with the LIGO-Virgo instruments.

I. INTRODUCTION

The Advanced LIGO (aLIGO) observatories completed their first observing run "O1" early-2016, operating at a factor of $3-4$ higher gravitational-wave (GW) strain sensitivity than their first-generation counterparts [1]. During O1, they made the first terrestrial observation of gravitational waves [2]. Emitted by a pair of coalescing black holes, these waves heralded an era of observational GW astrophysics as they traveled through Earth. Towards the end of this decade, we expect aLIGO to reach its design sensitivity. In addition to the US-based efforts, we also expect the French-Italian detector Advanced Virgo [3, 4], Japanese detctor KAGRA [5, 6], and LIGO-India [7] to begin observing at comparable sensitivities within a few years. With a global network of sensitive GW observatories, we can expect GW astronomy to face significant developments over the coming years.

Coalescing compact binaries of stellar-mass black holes (BH) and/or neutron stars (NS) are the primary targets for the second generation GW detectors [8–19]. A binary system of black holes was recently observed by aLIGO [2]. Previously, stellar-mass black holes had only been observed by inference in mixed binaries with stellar companion (through electromagnetic observations of the companion) [20–22]. Neutron stars, on the other hand, have had numerous sightings. Thousands of electromagnetically emitting neutron stars, or pulsars, have been documented [23], in varied situations: as radio pulsars [23, 24], in binary systems with a stellar companion [23–26], and in binary neutron stars (BNS) [23, 24, 27–29]. Mixed binaries of black holes and neutron stars, is an astrophysically interesting class of systems [16, 17, 30, 31], that has not yet been detected. We expect to observe $\mathcal{O}(10)$ mixed binaries per year with aLIGO [32].

NSBH binaries are of interest for multiple reasons. For instance, they have been long associated with (as possible progenitors of) short Gamma-ray Bursts (SGRBs) [33–41]. Depending on their equation of state (EoS), NSs can get disrupted by the tidal field of their companion BHs. Once disrupted, most of the NS material falls into the hole over an $\mathcal{O}(1{\rm ms})$ time-scale, with the rest partly getting ejected as unbound material and partly forming an accretion disk around the BH. This short lived $(0.1-1s)$ disk-BH system is hypothesized to drive SGRBs through the production of relativistic jets [39, 40, 42–45]. However, whether or not such a system forms depends also on the nature of the BH. Massive BHs (with $m_{\rm BH} \gtrsim 10M_\odot$), as well as BHs with large retrograde spins, tend to swallow the NS whole without forming a disk [46]. On the other hand, *low-mass* BHs with $m_{\rm BH} \in [3M_\odot, 8M_\odot]$, can disrupt their companion NSs much before merger, forming long-sustained disks that are required to sustain SGRBs [43, 47–49]. A *coincident* detection of both GWs

* prkumar@cita.utoronto.ca

and gamma-rays from an NSBH merger, will provide us with a unique opportunity to confirm this hypothesized link between NSBH mergers and GRBs [50].

Another question that compact object mergers can help answer is 'what is the nature of matter at nuclear densities supported by NSs'? A large fraction of past work aimed at measuring NS matter effects from GW signals has consisted of inquiries about BNSs [51–62]. In this paper, we will instead focus on NSBHs. During the course of early inspiral, the tidal field of the BH produces a deformation in its companion NS. The quadrupolar moment of the star associated with this deformation also depends on its material properties, through an EoS-dependent tidal deformability parameter $\Lambda_{\rm NS}$. This induced quadrupolar moment changes over the orbital time-scale, resulting in the emission of GWs in *coherence* with the orbital waves. These waves draw more energy from the orbit and increase the inspiral rate (as compared to an equivalent BBH) [63]. Closer to merger, the strong tidal field of the BH can disrupt the NS. The quadrupolar moment of the disrupted binary system falls monotonically over a millisecond time-scale [42, 43, 64–66], resulting in the damping of GW amplitude. This penultimate stage also depends strongly on the internal structure and energy transport mechanism of the NS, and carries the strongest tidal signature in the GW spectrum [44, 67].

Gravitational waves emitted by coalescing NSBH binaries carry subtle hints of the NS EoS from inspiral through to merger. During early inspiral, the tidal dephasing is relatively weak and appears as a 5^{th} Post-Newtonian (PN) order effect [68]. Closer to merger, a disruptive fate of the NS can result in a strong suppression of GW emission above a cut-off frequency [66]. Some past studies of tidal measurements with NSBH binaries have used PN inspiral-only waveforms [69]. In doing so, however, they ignore (i) the merger signal which could contain significant information for NSBHs, and (ii) the errors due to unknown vaccum terms in PN waveforms, which could dominate over the tidal terms themselves [70, 71]. Some other studies that account for merger effects via the use of complete numerical simulations [46], are limited in the binary parameter space they sample. Others, that do the same through the use of phenomenological waveform models [65, 72] use the Fisher matrix to estimate $\Lambda_{\rm NS}$ measurement errors. Fisher matrix estimates are known to be unreliable at realistic signal-to-noise ratios (SNR) [73], such as those as we might expect in the upcoming observing runs of GW detectors [32].

In this paper we study the measurability of neutron star's tidal deformability from realistic binaries of *low*-mass BHs and NSs by aLIGO. We also probe how tidal effects affect the estimation of other binary parameters for the same class of systems. This study improves upon previous work in the following ways. First, we include tidal effects during inspiral and merger in a consistent way, by using the waveform model of Lackey *et al.* [65] (abbreviated henceforth to "LEA"). Second, we include the effect of black hole spin on tidal GW signals, in addition to the effect of BH mass, tidal deformability of the NS, and the SNR. Third, we perform a complete Bayesian analysis, instead of using the Fisher matrix approximation. And fourth, we explore how our measurement errors decrease as we gain information from multiple (realistic) events.

We now outline the main questions and results discussed in this paper. First, we probe the effect of ignoring tidal effects in the recovery of non-tidal binary parameters, such as component masses and spins. This is the case for current and planned aLIGO efforts. To do so, we first use the enhanced-LEA (or "LEA+", see Sec. II A) model to generate a set of realistic signals; and then use non-tidal (BBH) waveform filters to estimate the underlying binary masses and spins with a Markov-chain Monte Carlo. Here and throughout, we use the zero-detuning high-power design sensitivity curve [1] to characterize the expected detector noise. We find that, for individual events, ignoring tidal effects will affect mass and spin-estimation only marginally; only for very loud signals (SNRs $\gtrsim 30$) will the systematic biases be large enough to exceed the underlying statistical uncertainty. Furthermore, detection searches can ignore tidal effects without loss of sensitivity.

Second, we study the ability of aLIGO to constrain neutron star tidal deformability with a single observation of an NSBH merger. For this, we use the same setup for signal waveforms as before, but replace the filter template model with one that includes tidal effects from inspiral through to merger (i.e. LEA+) [65]. For most binaries with BH masses outside of the mass-gap ($2-5M_{\odot}$) [74–77] and/or realistic signal-to-noise ratios (SNR), we find it difficult to put better than a factor of 2 bound on $\Lambda_{\rm NS}$ with a single observation. As we can see from Fig. 6, it is only at SNRs $\rho \gtrsim 20-30$ (under otherwise favorable circumstances, such as a stiff equation of state) that we are able to bring this down to a $\pm 75\%$ bound on $\Lambda_{\rm NS}$. For signals louder than $\rho = 30$, we can constrain $\Lambda_{\rm NS}$ to a much more meaningful degree (within $\pm 50\%$ of its true value). While this is discouraging at first, we turn to ask: what if we combine information from a population of low-SNR observations?

The EoS of matter at nuclear densities is believed to be universal among all neutron stars. The Tolman-Oppenheimer-Volkoff equation [78–80] would then predict that NS properties satisfy a universal relationship between $\Lambda_{\rm NS}$ and $m_{\rm NS}$. As the final part of this paper, we combine information from multiple observations of realistic NSBH systems and perform a fully-Bayesian analysis of how our estimation of $\Lambda_{\rm NS}$ changes as we accumulate detections. This is similar to an earlier study [81] aimed at binary neutron stars. We restrict ourselves to a population of NSs with masses clustered very tightly around $1.35M_{\odot}$ (with a negligible variance), and negligible spins. We sample different nuclear EoSs by sampling entire populations fixing different values for the NS tidal deformability. For all populations, we take source locations to be uniformly distributed in spatial volume,

and source orientations to be uniform on the 2−sphere. To summarize, we find the following: (a) Our median estimate for $\Lambda_{\rm NS}$ starts out prior dominated, but converges to within 10% of the true value within $10-20$ detections. (b) Measurement uncertainties for $\Lambda_{\rm NS}$, on the other hand, depend on $\Lambda_{\rm NS}$ itself. We find that for hard equations of state (with $\Lambda_{\rm NS} \geq 1000$), $10-20$ observations are sufficient to constrain $\Lambda_{\rm NS}$ within $\pm 50\%$. For softer equations of state, the same level of certainty would require substantially more $(25-40)$ observations. (c) Further, if the astrophysical "mass-gap" [74–77] is real, we find that $20-50\%$ additional observations would be required to attain the same measurement accuracy as above. And, (d) putting tighter constraints on the $\Lambda_{\rm NS}$ of a population would require 50+ NSBH observations, in any scenario. All of the above is possible within a few years of design aLIGO operation [82].

In this paper, we restrict our parameter space to span mass-ratios $q := m_{\rm BH}/m_{\rm NS} \in [2,5]$, BH spin (aligned with orbit) $\chi_{\rm BH} \in [-0.5,+0.75]$, and dimensionless NS tidal deformability $\Lambda_{\rm NS} := G\left(\frac{c^2}{G m_{\rm NS}}\right)^5 \lambda \in [500, 2000]$. These ranges are governed by the calibration of the LEA+ model which we use as filters. Most of the disruptive NSBH simulations that LEA+ has been calibrated to involve $1.35M_\odot$ NSs, and it is unclear how reliable the model is for different NS masses [65, 83]. This motivates us to conservatively fix NS masses to $1.35M_\odot$ in our simulated signals (not templates). But, since the domain of calibration of LEA+ excludes NS spin completely, we fix $\chi_{\rm NS} = 0$ in both signals as well as filter templates. We expect the effect of ignoring NS mass and spin variations in our NSBH populations to be less severe than for BNSs [84], considering the higher mass-ratios of NSBHs. The accuracy of our quantitative results depends on the reliability of LEA+, which is the only model of its kind in current literature. A more recent work [83] improves upon the amplitude description of LEA+, but needs to be augmented with a compatible phase model. Overall, we expect our broad conclusions here to hold despite modeling inaccuracies (with errors not exceeding $\mathcal{O}(10\%)$ [83]). Finally, our results apply to LIGO instruments at design sensitivity, which they are projected to attain by 2019 [1, 50].

The remainder of the paper is organized as follows. Sec. II discusses data analysis techniques and resources used in this paper, such as the waveform model, and parameter estimation algorithm. Sec. III discusses the consequences of ignoring tidal effects in parameter estimation waveform models. Sec. IV discusses the measurability for the leading order tidal parameter $\Lambda_{\rm NS}$ at plausible SNR values. Sec. V discusses the improvement in our measurement of $\Lambda_{\rm NS}$ with successive (multiple) observations of NSBH mergers. Finally, in Sec. VI we summarize our results and discuss future prospects with Advanced LIGO.

II. TECHNIQUES

A. Waveform Models

Lackey *et al.* (LEA) [65] developed a complete inspiral-merger waveform model for disrupting NSBHs. Theirs is a frequency-domain phenomenological model that includes the effect of BH and NS masses and spins $\{m_{\rm BH}, \chi_{\rm BH}, m_{\rm NS}\} \equiv \vec{\theta}$ and NS tidal deformability $\Lambda_{\rm NS}$. It was calibrated to a suite of 134 numerical relativity (NR) simulations of NSs inspiraling into spinning BHs. The parameter space these simulations span, which we assume to be the domain of validity for the LEA model, includes NS masses $1.2M_\odot \leq m_{\rm NS} \leq 1.45M_\odot$, mass-ratios $2 \leq q \leq 5$, and BH spins $-0.5 \leq \chi_{\rm BH} \leq +0.75$. They also sample a total of 21 two-parameter nuclear EoSs to cover the spectrum of NS deformability. The GW strain $\tilde{h}(f)$ per the LEA model can be written as

$$\tilde{h}_{\rm NSBH}(f, \vec{\theta}, \Lambda_{\rm NS}) = \tilde{h}_{\rm BBH}(f, \vec{\theta})\, A(f, \vec{\theta}, \Lambda_{\rm NS})\, e^{{\rm i}\Delta\Phi(f, \vec{\theta}, \Lambda_{\rm NS})}, \quad (1)$$

with NS spin $\chi_{\rm NS} = 0$ identically. Here, $\tilde{h}_{\rm BBH}$ is an underlying BBH waveform model. In the original LEA model, this was taken to be the SEOBNRv1 model [85] of the Effective-one-body (EOB) family [86]. The factor $A(\cdot)$ adjusts the amplitude of the BBH model to match that of an NSBH merger of otherwise identical parameters, with NS-matter effects parametrized by $\Lambda_{\rm NS}$. During early inspiral this term is set to unity, but is a sensitive function of $\Lambda_{\rm NS}$ close to merger. The term with $\Delta\Phi$ corrects the waveform phasing. During inspiral, $\Delta\Phi$ is set to the PN tidal phasing corrections, at the leading and next-to-leading orders [68]; close to merger, additional phenomenological terms are needed. Both A and $\Delta\Phi$ are calibrated to all 134 available NR simulations.

In this paper we use LEA for our signal and template modeling, but switch the underlying BBH model to SEOBNRv2 (and refer to it as enhanced-LEA or "LEA+") [87]. We using the reduced-order frequency-domain version of SEOBNRv2, which has the additional benefit of reducing computational cost [88]. We expect this enhancement from LEA→LEA+ to make our conclusions more robust because: (a) the SEOBNRv2 model is more accurate [89, 90], and (b) the differences between the two EOB models are caused by the inaccuracies of SEOBNRv1 during the *inspiral* phase, many orbits before merger [89]. Since LEA only augments inspiral phasing with PN tidal terms, our change in the underlying BBH model does not change LEA's construction, *and* increases the overall model accuracy during inspiral. Finally, we note that we approximate the full GW signal with its dominant $l = |m| = 2$ modes, that are modeled by LEA+. For use in future LIGO science efforts, we have implemented the LEA+ model in the LIGO Algorithms Library [91].

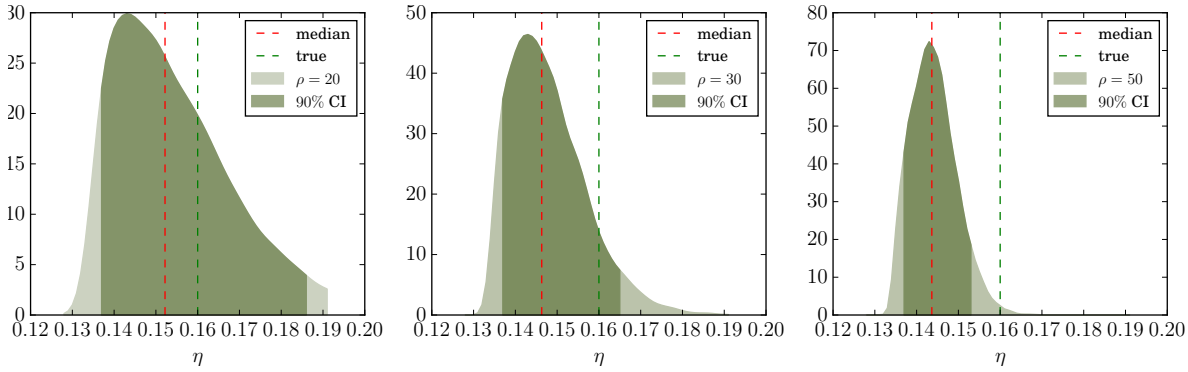

FIG. 1. **Illustrative posterior probability distributions for mass-ratio η at different SNR values:** We show here probability distributions for mass ratio η as measured for the same signal at different SNRs. The intrinsic parameters of the source are: $q = m_{\rm BH}/m_{\rm NS} = 5.4M_\odot/1.35M_\odot = 4$, $\chi_{\rm BH} = +0.5$, and $\Lambda_{\rm NS} = 2000$; and the signal is injected at SNRs $\rho = \{20, 30, 50\}$ (left to right). The templates *ignore* tidal effects. In each panel: the dashed red line marks the median value $\eta^{\rm Median}$, while the dashed green line show the true value $\eta^{\rm Injected}$. The darker shading shows the recovered 90% credible interval for η, $(\Delta\eta)^{90\%}$. Comparing systematic and statistical errors, we find that: at $\rho = 20$, η measurement is dominated by statistical errors; at $\rho = 30$, the two become comparable; and for louder signals ($\rho \simeq 50$), the systematic errors dominate.

B. Bayesian methods

The process of measuring systematic and statistical measurement errors involves simulating many artificial GW signals, and inferring source binary parameters from them using Bayesian statistics. We start with generating a signal waveform, using the model LEA+, and injecting it in zero noise to obtain a stretch of data d_n. Source binary parameters $\vec{\Theta} := \vec{\theta} \cup \{\Lambda_{\rm NS}\}$ are reconstructed from this injected signal. Using Bayes' theorem, their joint inferred probability distribution of $\vec{\Theta}$ can be written as

$$p(\vec{\Theta}|d_n, H) = \frac{p(d_n|\vec{\Theta}, H)\, p(\vec{\Theta}|H)}{p(d_n|H)}. \qquad (2)$$

Here, $p(\vec{\Theta}|H)$ is the *a priori* probability of binary parameters $\vec{\Theta}$ taking particular values, given H - which denotes all our collective knowledge, except for expectations on binary parameters that enter our calculations explicitly. Throughout this paper, we impose a prior that is uniform in individual component masses, BH spin, and the tidal deformability of the NS. In addition, we restrict mass-ratios to $q \geq 2$, as LEA+ is not calibrated for $1 \leq q \leq 2$. $p(d_n|\vec{\Theta}, H)$ is the likelihood of obtaining the given stretch of data d_n if we assume that a signal parameterized by $\vec{\Theta}$ is buried in it, and is given by

$$p(d_n|\vec{\Theta}, H) \equiv \mathcal{L}(\vec{\Theta}) = \mathcal{N} \exp[-\langle d_n - h|d_n - h\rangle], \qquad (3)$$

where $h \equiv h(\vec{\Theta})$ is a filter template with parameters $\vec{\Theta}$, $\langle\cdot|\cdot\rangle$ is a suitably defined detector-noise weighted inner-product [1], and $\mathcal{N}$ is an SNR-dependent normalization constant. As in Ref. [92] we use a likelihood that is maximized over over the template norm and we ignore extrinsic parameters that only enter in the template norm such as distance, orientation and sky location. In addition, we also maximize over coalescence time and phase. The denominator in Eq. 2 is the *a priori* probability of finding the particular signal in d_n and we assume that each injected signal is as likely as any other. Having constructed the probability distribution function $p(\vec{\Theta}|d_n, H)$, extracting the measured probability distribution for a single parameter (say α) involves integrating

$$p(\alpha|d_n, H) = \int {\rm d}\vec{\Theta}_\alpha\, p(\vec{\Theta}|d_n, H), \qquad (5)$$

where $\vec{\Theta}_\alpha$ is the set of remaining parameters, i.e. $\vec{\Theta}_\alpha := \vec{\Theta} - \{\alpha\}$.

We use the ensemble sampler Markov-chain Monte-Carlo algorithm implemented in the `emcee` package [93], to sample the probability distribution $p(\vec{\Theta}|d_n, H)$. We run 100 independent chains, each of which is allowed to collect 100, 000 samples and combine samples from chains that have a Gelman-Rubin statistic [94] close to unity. This procedure yields about 10,000 independent samples. One simplification we make to mitigate computational cost is to set the frequency sampling interval to $\Delta f = 0.4$ Hz, which we find to be sufficient for robust likelihoods calculations in zero noise [92]. We integrate Eq. 5 to obtain marginalized probability distributions for the NS tidal deformability parameter: $p(\Lambda_{\rm NS}|d_n, H)$. We will quote the median value of this distribution as our *measured* value for $\Lambda_{\rm NS}$, and the 90% credible intervals

[1] The inner product $\langle\cdot|\cdot\rangle$ is defined as [1]

$$\langle a|b\rangle \equiv 4\,{\rm Re}\left[\int_0^\infty \frac{\tilde{a}(f)\tilde{(b)}(f)^*}{S_n(|f|)}\,{\rm d}f\right], \qquad (4)$$

where $\tilde{a}(f)$ is the Fourier transform of the finite time series $a(t)$, and $S_n(|f|)$ is the one-sided amplitude spectrum of detector noise.

associated with the distribution as the statistical errorbars.

III. HOW IS PE AFFECTED IF WE IGNORE NS MATTER EFFECTS?

Past (and future) efforts with Advanced LIGO have used (or plan to use) BBH waveform templates to search for and characterize NSBH sources. In doing so, they ignore the signature of NS tidal effects on the emitted GWs. In this section we present a fully Bayesian analysis of the effect of this simplification on the recovery of non-tidal parameters from NSBH signals.

We inject LEA+ NSBH signals into zero noise, and run an MCMC sampler on them using equivalent BBH templates (same model, tidal terms $\to$ 0). We fix $m_{\rm NS} = 1.35M_\odot$ and $\chi_{\rm NS} = 0$, and explore a range of NS equations of state via the single tidal deformability parameter $\Lambda_{\rm NS} \in \{500, 800, 1000, 1500, 2000\}$. Our injections also span a rectangular grid in the BH parameter space, with vertices at $q \in \{2, 3, 4, 5\}$, i.e. $m_{\rm BH} \in \{2.7M_\odot, 4.05M_\odot, 5.4M_\odot, 6.75M_\odot\}$, and BH spins $\chi_{\rm BH} \in \{-0.5, 0, +0.5, +0.75\}$. Finally, we sample all other source-related parameters, that determine the signal strength but not character[2], by sampling the SNR $\rho \in \{20, 30, 50, 70\}$. Our choice of injection parameters here is motivated by two factors: (i) previous studies of the signatures of NS tidal effects on gravitational waves [46, 67, 97] (which suggest that necessary conditions for the observation of tidal effects with aLIGO include high SNRs and a low-mass spinning companion BH); and (ii) technical constraints of our chosen LEA+ model [65]. At design sensitivity, if we expect $0.2 - 300$ NSBH detections a year [82], we can expect to see $0.02 - 25$ *disruptive*[3] NSBH mergers a year, of which we will have $0.005 - 7$ observations with $\rho \geq 20$, and $0.002 - 3$ a year with $\rho \geq 30$. Therefore, our injection parameters span a physically interesting subset of NSBH binaries, that is *also* likely observable in the near future. For our Bayesian priors, we choose uniform distributions for both component masses and black hole spin: $m_{\rm BH} \in [1.2, 25]M_\odot$; $m_{\rm NS} \in [1.2, 3]M_\odot$; and $-0.75 \leq \chi_{\rm BH} \leq +0.75$.

The effect of ignoring tidal corrections in templates will manifest as a systematic shift of recovered median parameter values away from what they would be if we had used tidal templates with identical priors. In zero noise, we expect the probability distributions recovered using tidal templates to be multi-dimensional Gaussians with the maximum likelihood parameter values approaching their true values. If the priors are not restrictive, we expect the recovered median to also converge to the true value. However, the LEA model imposes significantly more restrictive priors (both mass-ratio and spin) than SEOBNRv2 [65, 87], which shifts the median value of parameters recovered using *our* tidal templates away from their true value. If we use LEA+ priors for our non-tidal templates, it would add a caveat to our original question 'can we estimate non-tidal NSBH parameters with equivalent BBH templates'. Instead, we approximate the median tidally recovered parameters by their true injected values, as one would expect to recover with an ideal model for tidally disruptive NSBH mergers. With this caveat, we estimate *systematic* measurement bias/errors as the differences between median and *injected* parameter values. As an illustration, in Fig. 1 we show the recovered probability distributions for binary mass ratio η for three NSBH injections, with $\rho = 20$ (left), 30 (middle), and $\rho = 50$ (right), and other parameters held fixed ($m_{\rm NS} = 1.35M_\odot$, $\chi_{\rm NS} = 0$, $m_{\rm BH} = 5.4M_\odot$, $\chi_{\rm BH} = +0.5$ and $\Lambda_{\rm NS} = 2000$). In each panel, both the *true* and median values of η are marked, and we use the shift between the red and green vertical lines as our estimate of systematic measurement errors. Darker shading in all panels marks 90% credible intervals, whose width $(\Delta\eta)^{90.0\%}$ we use as a direct measure of our *statistical* measurement uncertainty/error[4]. For the illustrated binary, we see clearly that even when the signal is moderately loud, with $\rho = 20$, statistical errors dominate over systematics for η. As we turn up the SNR further, the two error sources become comparable at $\rho \sim 30$, and systematic errors dominate finally when $\rho \simeq 50$.

Credible intervals $(\Delta X)^{90\%}$ showing the precision with which $X = \{\mathcal{M}_c, \eta, \chi_{\rm BH}\}$ can be measured, are presented in Appendix A. We remind ourselves that this *precision* is only meaningful so long as the measurement is *accurate* to begin with. Therefore, we define $\mathtt{R}_X$ as the ratio between systematic and statistical errors associated with the measurement of parameter X,

$$\mathtt{R}_X = \frac{(X^{\rm Median} - X^{\rm Injected})}{(\Delta X)^{90\%}}, \tag{6}$$

in order to compare the relative magnitude of both. Only when $|\mathtt{R}_X| \ll 1$ can we ignore tidal effects in our templates without hampering the measurement of non-tidal parameters from NSBH signals. When $\mathtt{R}_X$ approaches a few tens of percent of unity, we can begin to favor tidal templates for NSBH studies.

We start with calculating $\mathtt{R}_{\mathcal{M}_c}$ as a function of various source parameters and show it in Fig. 2. $\mathcal{M}_c$ is

[2] For aligned-spin signals and aligned-spin templates both, we only consider the contribution of the dominant $l = |m| = 2$ waveform multipoles. This approximation has the additional benefit of combining the dependence of the waveforms on inclination, polarization and sky location angles, as well as on distance, into the luminosity or *effective* distance. This quantity only appears as an overall scaling factor, and therefore only affects signal strength [96].

[3] We assume here that BH mass values are *uniformly* likely from $2M_\odot$ to $\sim 35M_\odot$ [2], but NSs are disrupted in NSBH mergers only if $q \leq 6$ and $\chi_{\rm BH} \geq 0$ [46, 67].

[4] We generalize the notation $(\Delta X)^{90.0\%}$ to mean the 90% credible interval width for any measured source parameter X.

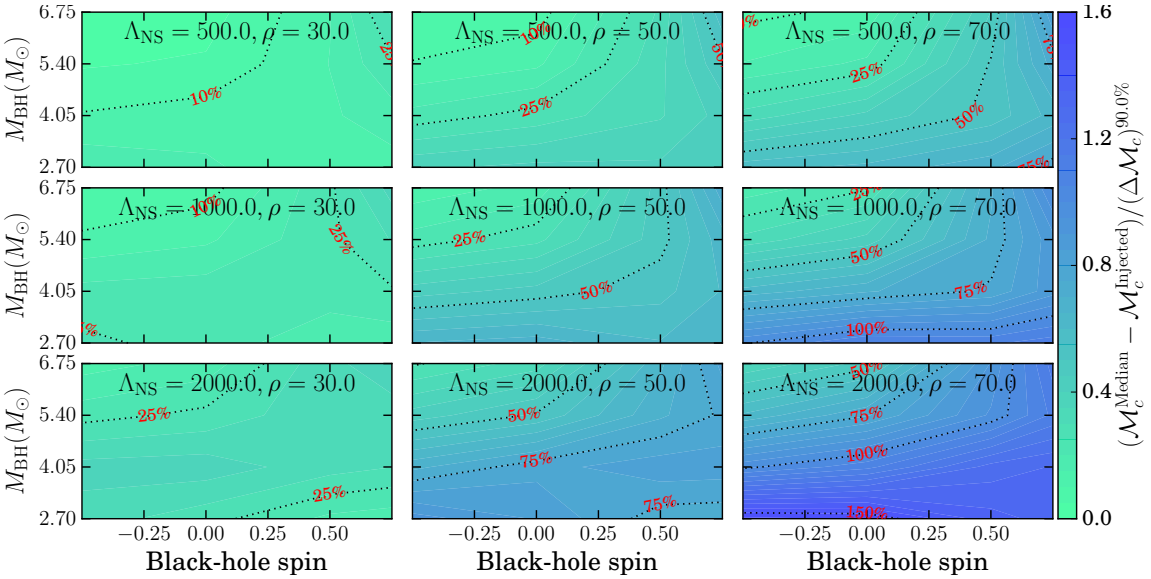

FIG. 2. **Ratio of systematic to statistical errors in measuring $\mathcal{M}_c$, ignoring tidal effects:** We show here the ratio of systematic and statistical measurement uncertainties for the binary chirp mass over the NSBH parameter space. Each panel shows the same as a function of BH mass and spin. NS mass is fixed at $m_{\rm NS} = 1.35M_\odot$, and its spin is set to zero. Down each column, we can see the effect of the increasing tidal deformability of the NS at fixed SNR. Across each row, we can see the effect of increasing the signal strength (SNR), with the tidal deformability of the NS fixed. We show dashed contours for $\mathtt{R}_{\mathcal{M}_c} = 10\%, 25\%, 50\% \cdots$, with interleaving filled color levels separated by 5%. For BBHs, the statistical errors dominate systematic ones for contemporary waveform models [90, 95]. We find that its not much different for NSBH binaries, until we get to very high SNRs $\rho \gtrsim 70$.

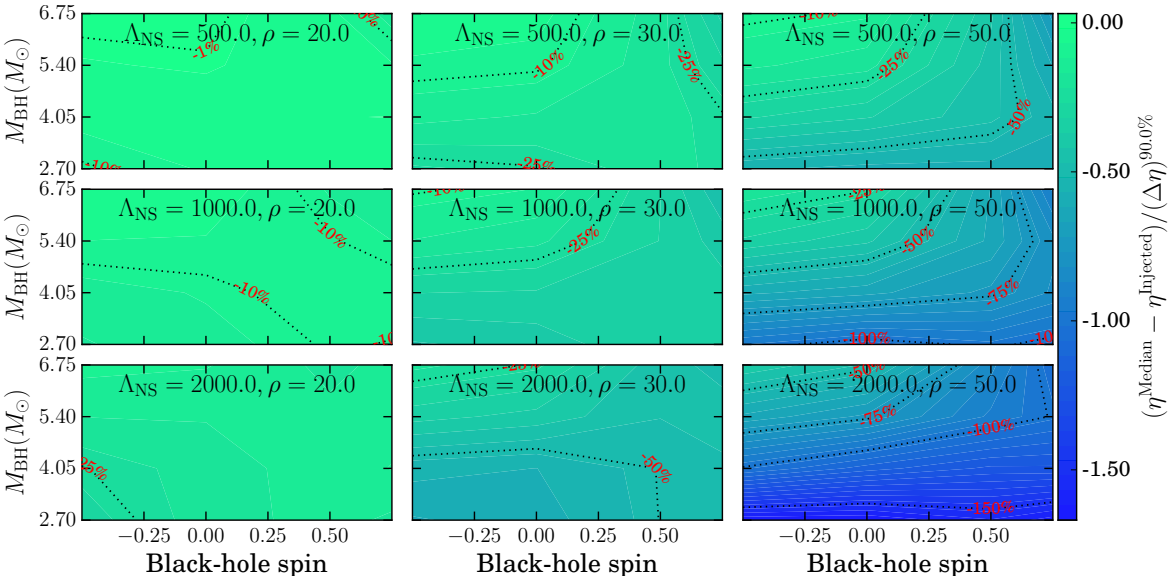

FIG. 3. **Ratio of systematic to statistical errors in measuring η, ignoring tidal effects:** This figure is similar to Fig. 2 with the difference that here we show the ratio of systematic and statistical error sources for the symmetric mass-ratio η and not chirp mass. We find that for fairly loud GW signals, at $\rho \simeq 50$, not including the effects of tidal deformation of the NS on GW emission can become the dominant source of error for astrophysical searches with Advanced LIGO. However, for quieter signals with $\rho \leq 30$, it will have a negligible effect on the measurement of η. We remind the reader that the SNRs here are always single detector values.

the leading order mass combination that affects the GW strain emitted by compact binaries as they spiral in, and is therefore determined the most precisely. We notice immediately that for $\rho \leq 30$ the systematics are well under control and we can obtain reliable chirp mass estimates for NSBH signals using BBH templates. For louder and

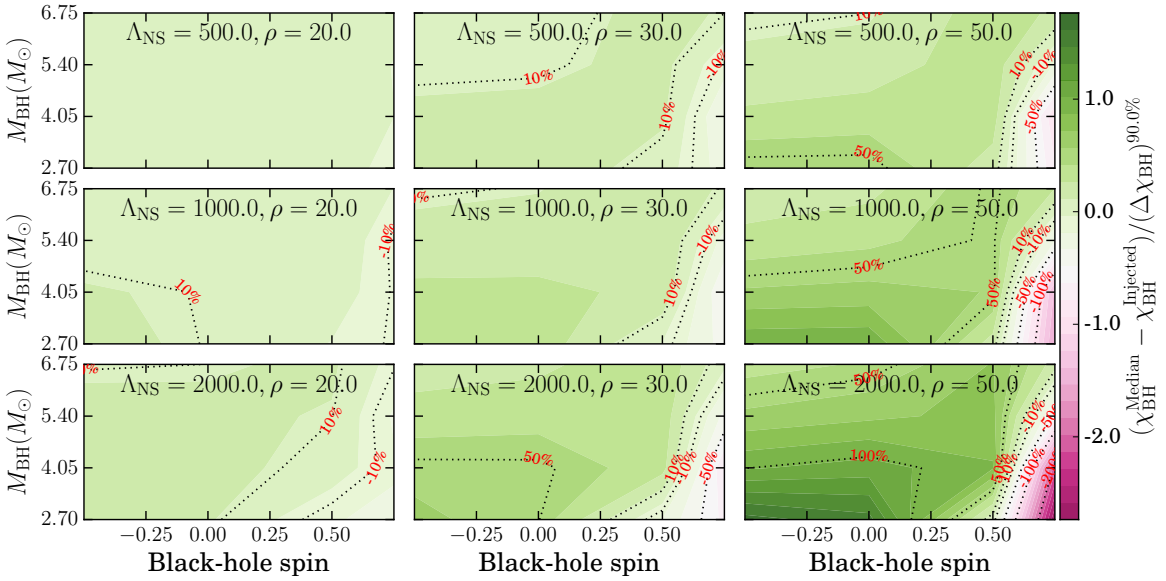

FIG. 4. **Ratio of systematic to statistical errors in measuring $\chi_{\rm BH}$, ignoring tidal effects:** This figure shows the ratio of the systematic and statistical measurement errors for BH spins $\mathtt{R}_{\chi_{\rm BH}}$. Information is arranged identically to Fig. 2, and 3, with the level spacing of filled contours increased to 15%. Similar to the case of mass parameters, we find that below $\rho \approx 30$, ignoring tidal effects in templates introduces minor systematic effects, which remain sub-dominant to the statistical measurement uncertainties.

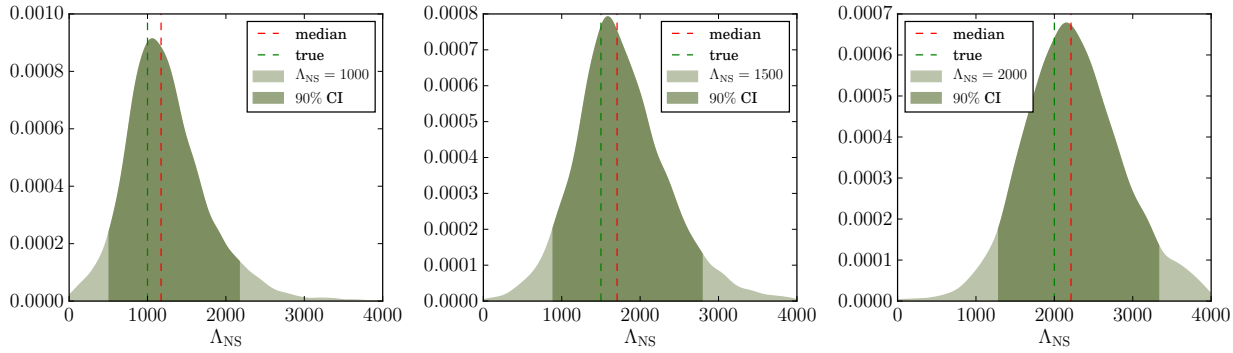

FIG. 5. **Illustrative posterior probability distributions for NS tidal deformability $\Lambda_{\rm NS}$:** We show here probability distributions recovered for the NS tidal deformability parameter $\Lambda_{\rm NS}$ from three GW injections, with parameters: $q = m_{\rm BH}/m_{\rm NS} = 5.4M_\odot/1.35M_\odot = 4$, $\chi_{\rm BH} = +0.5$, and $\Lambda_{\rm NS} = \{1000, 1500, 2000\}$ from left to right. The injection SNR is fixed at $\rho = 50$. The templates *include* tidal effects, with a prior $0 \leq \Lambda_{\rm NS} \leq 4000$. In each panel- the dashed red line marks the median value for $\Lambda_{\rm NS}$, and the dashed green line marks its *true* value. The darker shading shows the 90% credible interval, whose width $(\Delta\Lambda_{\rm NS})^{90\%}$ is a direct measure of our statistical uncertainty. By comparing the measurement uncertainty for these three injections, we see that $(\Delta\Lambda_{\rm NS})^{90\%}$ grows very slowly with $\Lambda_{\rm NS}$. Therefore, the fractional measurement error - $(\Delta\Lambda_{\rm NS})^{90\%}/\Lambda_{\rm NS}$ - decreases monotonically as $\Lambda_{\rm NS}$ increases (with signal strength fixed).

less likely SNRs ($\rho \simeq 50$), we find that $\mathtt{R}_{\mathcal{M}_c}$ can become comparable to unity, but only if the BH has prograde spin $\chi_{\rm BH} \gtrsim 0.4$, *and* the true NS tidal deformability is large enough, s.t. $\Lambda_{\rm NS} \gtrsim 1000$. We therefore conclude that only for very loud signals, with $\rho \gtrsim 50 - 70$, will the inclusion of tidal terms in template models improve $\mathcal{M}_c$ estimation. For lower SNRs, inclusion of new physical content in templates will instead get washed out by detector noise. In addition, we also note that $\mathtt{R}_{\mathcal{M}_c} \geq 0$ always, i.e. $\mathcal{M}_c$ is always being over-estimated. This is to be expected since the tidal deformation and disruption of NSs close to merger reduces GW signal power at high frequencies, making the resulting signal resemble a BBH signal of lower merger frequency - and therefore of higher mass.

Next, in Fig. 3, we show the ratio of measurement errors $\mathtt{R}_\eta$ for the symmetric mass-ratio. Going through the figure from left to right, we find that for realistic SNRs ($\rho \leq 30$) the systematics remain below statistical errors for η measurement. The worst case is of the most deformable NSs ($\Lambda_{\rm NS} = 2000$), but even for them systematics in η are $2\times$ smaller than the statistical measurement

errors. Moving to louder signals with $\rho \simeq 50$, we find that for binaries of fairly deformable NSs ($\Lambda_{\rm NS} \gtrsim 1500$) and low-mass BHs ($m_{\rm BH} \leq 5M_\odot$) that have prograde spins ($\chi_{\rm BH} \gtrsim +0.4$), our measurement of mass-ratio can be seriously compromised by ignoring tidal physics in template models. This pattern is continued at even higher SNRs, as we can see from Fig. 3. We therefore conclude that, even if under moderate restrictions on BH and NS parameters, $\rho = 30 - 50$ is loud enough to motivate the use of tidal templates in aLIGO data analyses. In addition, we also notice that, unlike for $\mathcal{M}_c$, the median value of η is always *lower* than its true value, which is what we expect if we want BBH templates to fit NSBHs that disrupt and merge at lower frequencies.

Moving on from mass to spin parameters, we now consider the measurement of BH spin angular momentum $\chi_{\rm BH}$. The ratio of systematic and statistical errors for $\chi_{\rm BH}$ are shown in Fig. 4. The presentation of information in this figure is identical to that of Fig. 2 and 3. A diverging colormap is used so that both extremes of the colorbar range point to large systematic biases, while its zero (or small) value lies in the middle. For the lowest SNR considered ($\rho = 30$), $\chi_{\rm BH}$ bias is about $2\times$ smaller than its statistical measurement uncertainty, and is therefore mostly negligible. Both do become somewhat comparable, but only when we have the most deformable NSs in orbit around low-mass BHs. At higher SNRs ($\rho \simeq 50 - 70$), we find that the systematics in $\chi_{\rm BH}$ measurement can dominate completely, especially for binaries containing mass-gap violating BHs and/or deformable NSs with $\Lambda_{\rm NS} \geq 1000$. From Fig. 4 we additionally note that when the source spin magnitudes approach the highest allowed, i.e. at both extremes of the x-axes, $\chi_{\rm BH} \times \mathtt{R}_{\chi_{\rm BH}} < 0$. This is to be expected because the median of the recovered posterior distributions for $\chi_{\rm BH}$ can only get pushed inwards from the boundaries.

Summarizing these results, we find that irrespective of system parameters, below a signal-to-noise ratio of 30, our measurements of mass and spin parameters of astrophysical NSBH binaries will remain limited by the intrinsic uncertainty due to instrument noise, and do not depend on whether we include tidal effects in template models. However, when the signal-to-noise ratio exceeds 30 the systematic bias in binary mass and spin measurements become comparable to and can exceed the uncertainty due to noise. Of the different non-tidal parameters considered, we find that the measurement of η degrades worst (in a relative-error sense) due to the use of BBH templates in deciphering an NSBH signal. Of all the sub-categories, we find that tidal templates could especially help with the parameter estimation of astrophysical *mass-gap violating* NSBH binaries,

IV. WHAT DO WE GAIN BY USING TEMPLATES THAT INCLUDE NS MATTER EFFECTS?

In the previous section, we showed that the effects of the tidal deformation of NSs by their companion BHs become discernible in the GW spectrum under certain favorable conditions, including (a) BH mass is sufficiently small, (b) BH spin is positive aligned, i.e. $\chi_{\rm BH} \gtrsim +0.4$, (c) the NS is not very compact, with $\Lambda_{\rm NS} \gtrsim 1000$, and (d) the source location and orientation are such that its GW SNR $\gtrsim 30$. Both condition (a) and (b) enhance the tidal distortion of the star and increase the number of orbits the system goes through at small separation, where the differences between NSBH and BBH signals are maximal. Conditions (a)-(c) also reduce the onset frequency of the disruption of the NS, allowing for it to happen earlier in the orbit. We expect that these conditions are also the ones which should maximize the likelihood of *measuring* tidal effects in NSBH signals. Here, we turn the question around to ask: under similarly favorable circumstances, can we gain insights about the internal structure of neutron stars from GW observations?

In this section, we calculate the accuracy with which we measure $\Lambda_{\rm NS}$ from *single* GW observations. We sample the same set of disruptive NSBH mergers as in the previous section, i.e. those with $q = \{2, 3, 4, 5\}$, $\chi_{\rm BH} = \{-0.5, 0, +0.5, +0.75\}$, and $\Lambda_{\rm NS} = \{500, 800, 1000, 1500, 2000\}$; fixing the NS mass $m_{\rm NS} = 1.35M_\odot$ and $\chi_{\rm NS} = 0$. For each unique combination of these parameters, we inject LEA+ signals into zero noise and perform a fully Bayesian parameter estimation analysis of each with LEA+ templates. Our priors on component masses and spins remain as in the previous section, with mass-ratio additionally restricted to $2 \leq q \leq 6$, and $\Lambda_{\rm NS}$ sampled uniformly from $[0, 4000]$. As an illustration of individual injections, we show the recovered probability distribution for $\Lambda_{\rm NS}$ for three specific configurations in Fig. 5. We fix $q = m_{\rm BH}/m_{\rm NS} = 5.4M_\odot/1.35M_\odot = 4$, with $\chi_{\rm BH} = +0.5$, and vary $\Lambda_{\rm NS}$ over $\{1000, 1500, 2000\}$ between the three panels. The SNR is fixed at $\rho = 50$. The darker shaded regions mark the 90% credible interval on $\Lambda_{\rm NS}$. We note that $\Lambda_{\rm NS}$ is estimated to within ± 2000 of its true value at this SNR. Another interesting thing to note is that while $(\Delta\Lambda_{\rm NS})^{90\%}$ slowly grows with $\Lambda_{\rm NS}$, the fractional uncertainty

$$\delta\Lambda_{\rm NS}^{90\%} := (\Delta\Lambda_{\rm NS})^{90\%}/\Lambda_{\rm NS} \tag{7}$$

decreases instead. Further illustrations, showing the correlation between tidal and non-tidal parameters, are presented in Appendix B. We will continue here to focus on the measurement of $\Lambda_{\rm NS}$ itself.

In Fig. 6 we show the main results of this section. In each panel, as a function of black hole mass and spin, we show the measured 90% credible interval widths $(\Delta\Lambda_{\rm NS})^{90\%}$. These correspond to the full width of the dark shaded regions in the illustrative Fig. 5. The effect of increasing signal strength can be seen as we go

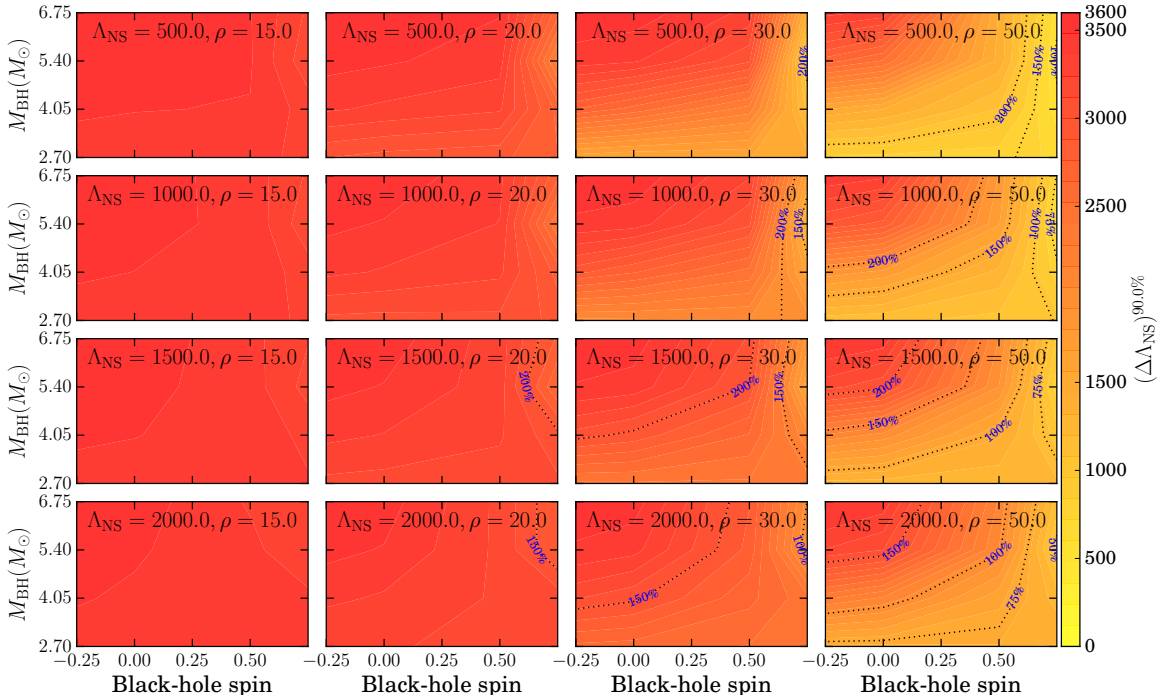

FIG. 6. **Statistical uncertainty in $\Lambda_{\rm NS}$ measurement:** Here we show the statistical uncertainty in the measurement of $\Lambda_{\rm NS}$. In each panel, the same is shown as a function of the BH mass and spin, keeping $\Lambda_{\rm NS}$ and injection's SNR ρ fixed (noted in the panel). Rows contain panels with the same value of $\Lambda_{\rm NS}$, with ρ increasing from left to right. Columns contain panels with the same value of ρ, with $\Lambda_{\rm NS}$ increasing from top to bottom. Contours at $(\Delta\Lambda_{\rm NS})^{90\%} = \{50\%, 75\%, 100\%, 150\%, 200\%\} \times \Lambda_{\rm NS}^{\rm Injected}$ demarcate regions where we can constrain the $\Lambda_{\rm NS}$ parameter well (within a factor of two of the injected value). We note that, as expected, the measurement accuracy for $\Lambda_{\rm NS}$ improves with (i) increasing SNR, (ii) increasing $\Lambda_{\rm NS}$, (iii) increasing BH spin, and (iv) decreasing BH mass.

from left to right in each row. The effect of the NS tidal deformability parameter $\Lambda_{\rm NS}$ on its own measurability can be seen by comparing panels within each column, with the NS becoming more deformable from top to bottom. A uniform pattern emerges in the left-most column, which corresponds to $\rho = 20$. We find that at this signal strength, our measurement of $\Lambda_{\rm NS}$ is dominated by the width of our prior on it. The 90% credible intervals span the entire allowed range for $\Lambda_{\rm NS}$, making a reasonable estimation of $\Lambda_{\rm NS}$ at $\rho \simeq 20$ difficult. Increasing the signal strength to $\rho = 30$ gives marginally better results, bringing down the statistical uncertainties to within $\pm 75 - 100\%$ of the true $\Lambda_{\rm NS}$ value [5]. It is not until we reach an SNR as high as $\rho \gtrsim 50$, can we put meaningful (i.e. $\mathcal{O}(10\%)$) constraints on $\Lambda_{\rm NS}$. For e.g., with a *single* observation of a $q = 4$ binary with $\chi_{\rm BH} \geq 0.6$ and $\rho = 50$ [6], we would be able to estimate $\Lambda_{\rm NS}$ to within $\pm 40\%$ of its true value (which is equivalent to measuring the ratio of NS radius to mass with an uncertainty of about $\pm 10\%$). These results agree well with Sec. III, and are consistent with Fisher matrix estimates at high SNRs [65].

Amongst other source parameters, BH mass and spin play a dominant role. A smaller BH with a larger spin always allows for a more precise measurement on $\Lambda_{\rm NS}$. We can see this in the bottom right corner of each panel in Fig. 6, which corresponds to low-mass BHs with large spins, and is simultaneously the region of smallest measurement errors on $\Lambda_{\rm NS}$. The actual deformability of the NS also plays an important role on its own measurability. For e.g., when $\Lambda_{\rm NS} \leq 1000$, it is fairly difficult to meaningfully constrain $\Lambda_{\rm NS}$ without requiring the source to be close (≈ 100Mpc) with a GW SNR $\rho \gtrsim 50$. Quantifying this further, in Fig. 7 we show the minimum signal strength required to attain a certain level of credibility in our $\Lambda_{\rm NS}$ measurement, as a function of BH properties. The NS is allowed the most favorable (hardest) EoS considered, with $\Lambda_{\rm NS}^{\rm true} = 2000$. We first note that, even with the most favorable BH and NS properties, achieving a $\pm 50\%$ measurement certainty on $\Lambda_{\rm NS}$ will require a GW SNR $\rho \gtrsim 30$. If we additionally restrict BH masses to lie outside of the so-called astrophysical mass-gap [74–77], we will simultaneously need to restrict BH spins to $\chi_{\rm BH} \gtrsim +0.5$ to obtain the same measurement credibility at the same source location.

In summary, with a single moderately loud ($\rho \lesssim 30$)

[5] The symmetric error-bars of $\pm$X% correspond to $\delta\Lambda_{\rm NS}^{90\%} = 2$X%.
[6] For an optimally oriented source with $q = 4, m_{\rm NS} = 1.35 M_\odot, \chi_{\rm BH} = 0.6$, an SNR of $\rho = 50$ corresponds to a luminosity distance of ≈ 113Mpc.

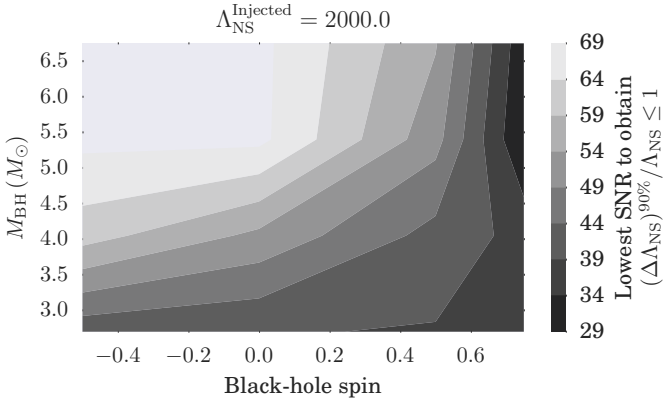

FIG. 7. We show here, as a function of BH mass and spin, the *minimum* signal strength (SNR) required to constrain $\Lambda_{\rm NS}$ within an interval of width equal to 100% of its true value, i.e. with $\pm 50\%$ error-bars. The NS mass is fixed at $1.35 M_\odot$, spin at zero, and $\Lambda_{\rm NS} = 2000$. We can see that, even in the most conducive circumstances with large aligned $\chi_{\rm BH}$ and a comparable mass BH, we can only constrain $\Lambda_{\rm NS}$ to better than $\pm 50\%$ *if* the SNR is $\gtrsim 29$. In the era of design sensitivity LIGO instruments, we expect this to happen approximately once in a year of observation [82].

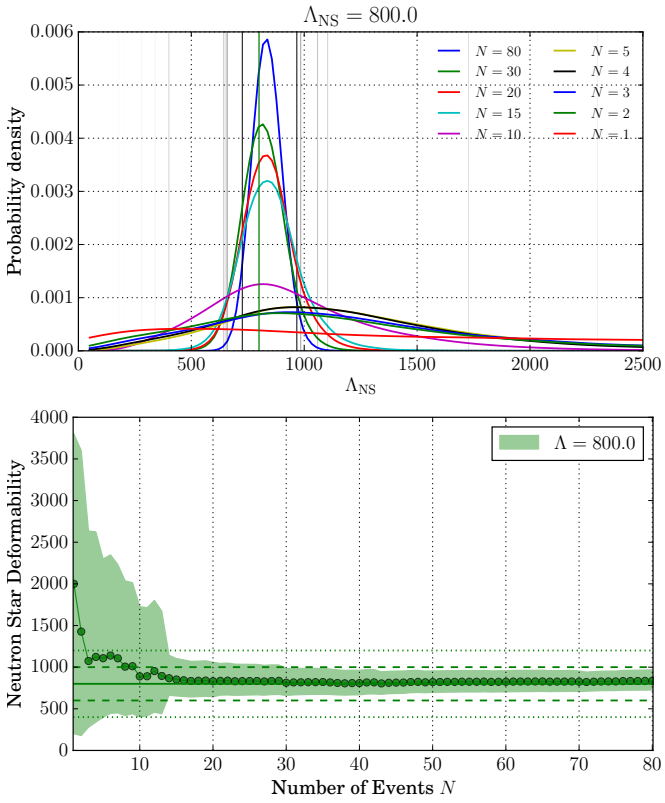

FIG. 8. **Recovery of $\Lambda_{\rm NS}$ for an increasingly large population of BH-NS signals.** *Top*: Posterior probability distributions for $\Lambda_{\rm NS}$ (colored curves), and associated 90% credible intervals (grey vertical lines), shown for different number of accumulated observations N. Distributions are normalized to unit area. *Bottom*: Measured median value of $\Lambda_{\rm NS}$ (as solid circles) and the associated 90% credible intervals (as the vertical extent of filled region), shown as a function of number of observations N. Solid horizontal line indicates the true value of $\Lambda_{\rm NS} = 800$. Dashed and dotted horizontal lines (a pair for each line-style) demarcate $\pm 25\%$ and $\pm 50\%$ error bounds.

GW signal from a disruptive BHNS coalescence, we can constrain the NS compactness parameter $\Lambda_{\rm NS}$ within $\pm 100\%$ of its true value. To measure better with one observation, we will need a more fine-tuned source, with $\rho \geq 30$ and high BH spins, or $\rho \geq 50$. Finally, we note that these results are *conservative*, and BHs with spins $\chi_{\rm BH} > 0.75$ will prove to be even more favorable laboratories for $\Lambda_{\rm NS}$ measurement. However, we are presently unable to explore this case in quantitative detail due to waveform model restrictions [65], which will also restrict our analyses of GW signals during the upcoming LIGO observing runs.

V. COMBINING OBSERVATIONS: LOOKING FORWARD WITH ADVANCED LIGO

In the previous section, we showed that single observations of NSBH coalescences at moderate SNRs have little information about the internal structure of neutron stars that will be accessible to Advanced LIGO at its design sensitivity. We expect all neutron stars to share the same equation of state, and hence the same $\Lambda_{\rm NS}(m_{\rm NS})$. In addition, we know that the mass distribution of (most) NSs that have not been spun up to millisecond periods (which are the ones we focus on in this paper, by setting $\chi_{\rm NS} \approx 0$) is narrowly peaked around $\sim 1.35 M_\odot$ [98]. Therefore, information from multiple NSBH observations can be combined to improve our estimation of $\Lambda_{\rm NS}$. We explore the same in this section within a fully Bayesian framework. We refer the reader to Ref. [60, 61, 99] for similar analyses of BNS inspirals.

An intuitive understanding of the problem is gained by considering first multiple *identical* sources with realistic but different SNRs. Let us consider the case of a population of optimally oriented binaries [7], distributed uniformly in spatial volume out to a maximum *effective* distance [8], $D^{\rm max}$. $D^{\rm max}$ is set by the minimum SNR threshold $\rho_{\rm min}$ at which a source is considered detectable [9]. Next, we divide this volume into I concentric

[7] An optimally oriented binary is one which is located directly overhead the detector, with the orbital angular momentum parallel to the line joining the detector to the source. Such a configuration maximizes the observed GW signal strength in the detector.

[8] *effective* distance D is a combination of distance to the source, its orientation, and its sky location angles; and has a one-to-one correspondence with SNR for non-precessing sources. This is so because for such sources, their location and orientation remain constant over the timescales within which they sweep through aLIGO's sensitive frequency band.

[9] which we take as $\rho_{\rm min} = 10$ throughout.

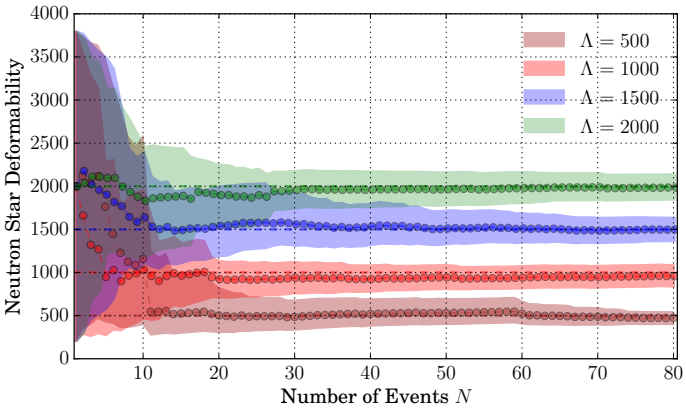

FIG. 9. **Improvement in $\Lambda_{\rm NS}$ measurement accuracy for different NS EoS:** In this figure, the filled regions show how our measurement of $\Lambda_{\rm NS}$ improves as the number of observed events (N, shown on x-axis) increases. Each color corresponds to an independent population with its true value of $\Lambda_{\rm NS}$ given in the legend. For each population, we show the median $\Lambda_{\rm NS}$ value (as filled circles), as well as the associated 90% credible intervals for the measurement (as the vertical extent of the filled region about the median), as functions of N.

shells, with radii D_i. If we have a measurement error σ_0 for $\Lambda_{\rm NS}$, associated with a source located at $D = D_0$, the same error for the same source located within the $i-$th shell would be $\sigma_i = \sigma_0 \frac{D_i}{D_0}$. Ref. [56] calculated that the combined error σ from N independent measurements of $\Lambda_{\rm NS}$ in such a setting to be

$$\frac{1}{\sigma^2} = \sum_{i=1}^{I} \frac{N_i}{\sigma_i^2} = \left(\frac{D_0}{\sigma_0}\right)^2 \sum_{i=1}^{I} \frac{N_i}{D_i^2} \qquad (8)$$
$$= \left(\frac{D_0}{\sigma_0}\right)^2 \int_0^{D^{\rm max}} \frac{4\pi D^2 n}{D^2} {\rm d}D = \left(\frac{D_0}{\sigma_0}\right)^2 \frac{3N}{(D^{\rm max})^2},$$

where N_i is the number of sources within the $i-$th shell (s.t. $N := \sum N_i$), and n is the number density of sources in volume. The root-mean-square (RMS) averaged measurement error from N sources is then [56]

$$\sigma_{avg} := \frac{1}{\sqrt{1/\sigma^2}} = \frac{\sigma_0}{D_0} D^{\rm max} \frac{1}{\sqrt{3N}}, \qquad (9)$$

given a fiducial pair (σ_0, D_0). It is straightforward to deduce from Eq. 9 that measurement uncertainty scales as $1/\sqrt{N}$, and the uncertainty afforded by a single observation with a high SNR ρ_c can be attained with $N = \rho_c^2/300$ realistic observations that have $\rho \geq \rho_{\rm min}$. E.g., to get to the level of certainty afforded by a single observation with $\rho = 70$, we would need $49/3 \approx 16-17$ realistic (low SNR) detections.

While we discussed Eq. 9 for a population of optimally oriented sources, it is valid for a more general population distributed uniformly in effective volume [56] ($\propto D^3$). However, it still only applies to sources with identical masses and spins, and we overcome this limitation by performing a fully Bayesian analysis next.

Astrophysical source population: Imagine that we have N stretches of data, $d_1, d_2, \cdots, d_N$, each containing a single signal emitted by an NSBH binary. Each of these signals can be characterized by the non-tidal source parameters $\vec{\theta} := \{m_{\rm BH}, m_{\rm NS}, \chi_{\rm BH}, \chi_{\rm NS}, \vec{\alpha}\}$, and $\{\Lambda_{\rm NS}\}$, where $\vec{\alpha}$ contains extrinsic parameters, such as source distance, inclination, and sky location angles. As before, let H denote all of our collective prior knowledge; for instance, H includes our assumption that all NSs in a single population have the same deformability parameter $\Lambda_{\rm NS}$, and that its cumulative measurement is therefore possible. The probability distribution for $\Lambda_{\rm NS}$, given N unique and independent events, is

$$p(\Lambda_{\rm NS}|\, d_1, d_2, \cdots, d_N, H)$$
$$= \frac{p(d_1, d_2, \cdots, d_N|\Lambda_{\rm NS}, H)\, p(\Lambda_{\rm NS}|H)}{\int p(\Lambda_{\rm NS}|H) p(d_1, d_2, \cdots, d_N|\Lambda_{\rm NS}, H) {\rm d}\Lambda_{\rm NS}}, \qquad (10)$$
$$= \frac{p(\Lambda_{\rm NS}|H) \prod_i p(d_i|\Lambda_{\rm NS}, H)}{\int p(\Lambda_{\rm NS}) p(d_1, d_2, \cdots, d_N|\Lambda_{\rm NS}, H) {\rm d}\Lambda_{\rm NS}}, \qquad (11)$$
$$= \frac{p(\Lambda_{\rm NS}|H) \prod_i \left(p(\Lambda_{\rm NS}|d_i, H) \frac{p(d_i)}{p(\Lambda_{\rm NS}|H)} \right)}{\int\, p(\Lambda_{\rm NS}|H)\, p(d_1, d_2, \cdots, d_N|\Lambda_{\rm NS}, H) {\rm d}\Lambda_{\rm NS}}; \qquad (12)$$

where Eq. 10 and Eq. 12 are application of Bayes' theorem, while Eq. 11 comes from the mutual independence of all events. Assuming in addition that all events are *equally likely*: $p(d_i) = p(d_j) = p(d)$, we get

$$p(\,\Lambda_{\rm NS}|d_1, d_2, \cdots, d_N, H)$$
$$= p(\Lambda_{\rm NS})^{1-N} \times \frac{p(d)^N}{\int p(\Lambda_{\rm NS}) p(d_1, d_2, \cdots, d_N|\Lambda_{\rm NS}, H) {\rm d}\Lambda_{\rm NS}}$$
$$\times \prod_i p(\Lambda_{\rm NS}|d_i, H), \qquad (13)$$

where the prior probability $p(\Lambda_{\rm NS}|H)$ is written $p(\Lambda_{\rm NS})$ for brevity. *A priori*, we assume that no particular value of $\Lambda_{\rm NS}$ is preferred over another within the range $[0, 4000]$, i.e.

$$p(\Lambda_{\rm NS}|H) = \frac{1}{4000} {\rm Rect}\left(\frac{\Lambda_{\rm NS} - 2000}{4000}\right). \qquad (14)$$

With a uniform prior, the first two factors in Eq. 13 can be absorbed into a normalization factor $\mathcal{N}$, simplifying it to

$$p(\Lambda_{\rm NS}|d_1, d_2, \cdots, d_N; H) = \mathcal{N} \prod_{i=1}^{N} p(\Lambda_{\rm NS}|d_i, H). \qquad (15)$$

In the second set of terms in Eq. 15 (of the form $p(\Lambda_{\rm NS}|d_i, H)$), each is the probability distribution for $\Lambda_{\rm NS}$ inferred *a posteriori* from the i-th observation by marginalizing

$$p(\Lambda_{\rm NS}|d_i, H) = \int p(\vec{\theta}, \Lambda_{\rm NS}|d_i, H)\, {\rm d}\vec{\theta}, \qquad (16)$$

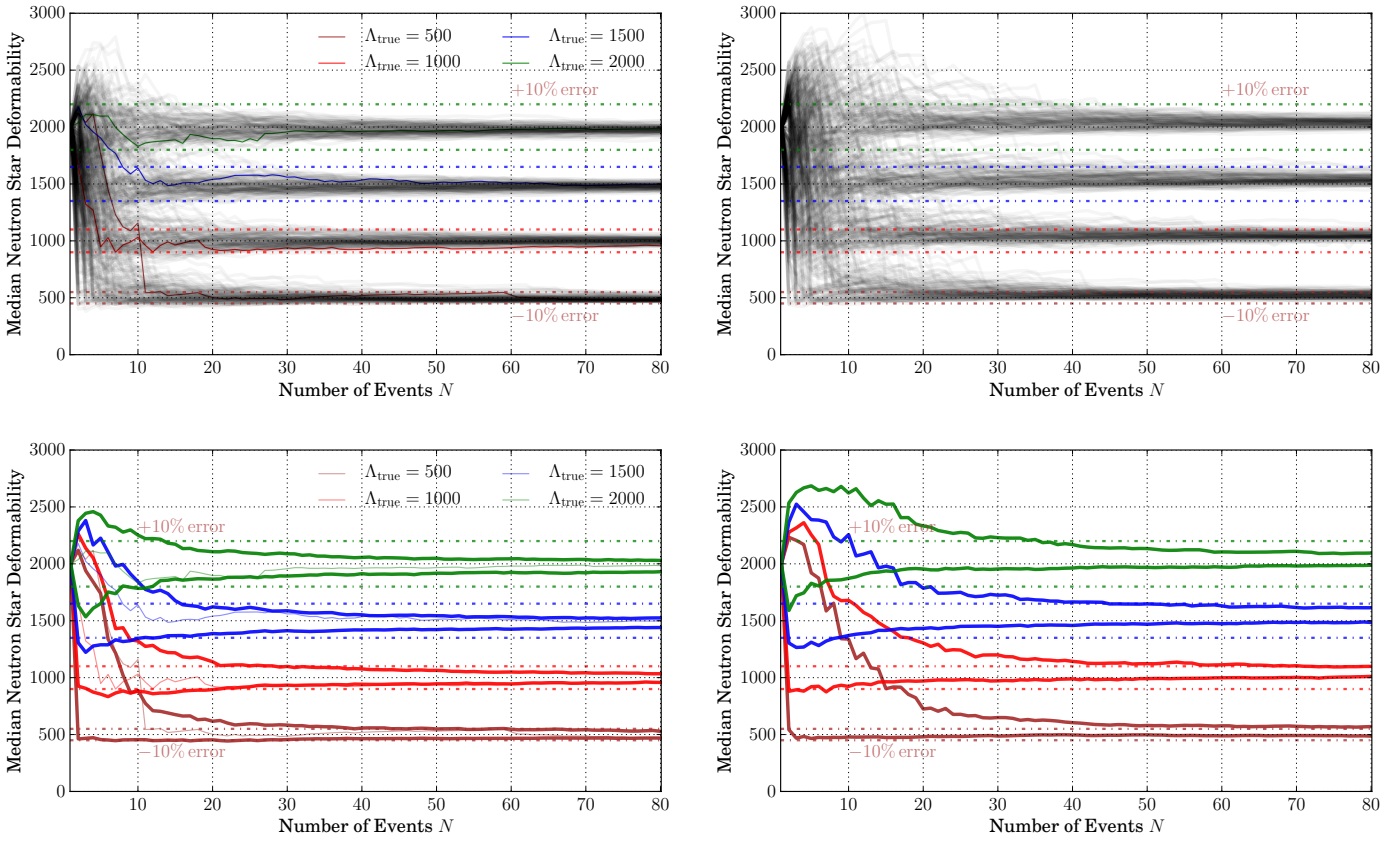

FIG. 10. **No Mass-Gap**, *top left*: The top figure shows the median value of the recovered probability distribution for $\Lambda_{\rm NS}$, as a function of the number of observed events N. There are four ensembles of curves, corresponding to $\Lambda_{\rm NS} = \{500, 1000, 1500, 2000\}$, with a hundred independent population draws within each ensemble. One curve in each ensemble is highlighted in color, representing the realizations already plotted in Fig. 9. In the same color we show $\pm 10\%$ error-bounds on $\Lambda_{\rm NS}$ with horizontal dash-dotted lines. **No Mass-Gap**, *bottom left*: Here we show the interval of $\Lambda_{\rm NS}$ values within which the median $\Lambda_{\rm NS}$ lies for 90% of the populations in each ensemble shown in the top left panel. We observe that within $10 - 25$ observations, the median of the measured cumulative probability distribution for $\Lambda_{\rm NS}$ converges to within 10% of its true value. **Mass-Gap**, *right column*: These panels are identical to their counterparts on the left, with the only difference that the BH masses in each population are restricted to lie *outside* the astrophysical mass-gap (i.e. paradigm B). The difference that we observe under this paradigm is that we need more (30+) events to achieve the same (10%) measurement accuracy for populations with $\Lambda_{\rm NS} < 1000$. For more deformable neutron stars, $10 - 25$ events would suffice.

where $p(\vec{\theta}, \Lambda_{\rm NS}|d_i, H)$ is the inferred joint probability distribution of all source parameters $\vec{\theta} \cup \{\Lambda_{\rm NS}\}$ for the i-th event, as given by Eq. 2. We note that Fig. 5 illustrates $p(\Lambda_{\rm NS}|d_i, H)$ for three individual events. By substituting Eq. 14-16 into Eq. 15, we calculate the probability distribution for $\Lambda_{\rm NS}$ as measured using N independent events.

Our goal is to understand the improvement in our measurement of $\Lambda_{\rm NS}$ with the number of recorded events. To do so, we simulate a population [10] of N events, and quantify what we learn from each successive observation using Eq. 15. This allows us to quantify how rapidly our median estimate for $\Lambda_{\rm NS}$ converges to the true value, and how rapidly our credible intervals for the same shrink, with increasing N. Finally, we generate and analyze an ensemble of populations in order to average over the stochastic process of population generation itself.

In order to generate each population, the first step is to fix the NS properties: (i) NS mass $m_{\rm NS} = 1.35 M_\odot$, (ii) NS spin $\chi_{\rm NS} = 0$ and (iii) NS tidal deformability $\Lambda_{\rm NS} =$ fixed value chosen from $\{500, 800, 1000, 1500, 2000\}$. Next, we generate events, by sampling BH mass (uniformly) from $m_{\rm BH} \in [3M_\odot, 6.75M_\odot]$, BH spin (uniformly) from $\chi_{\rm BH} \in [0, 1]$, orbital inclination from $\iota \in [0, \pi]$, and source location uniform in spatial volume[11].

[10] A population here is an ordered set of events, and an event itself is the set of parameters describing one astrophysical NSBH binary.

[11] with a minimum SNR $\rho_{\rm min} = 10$

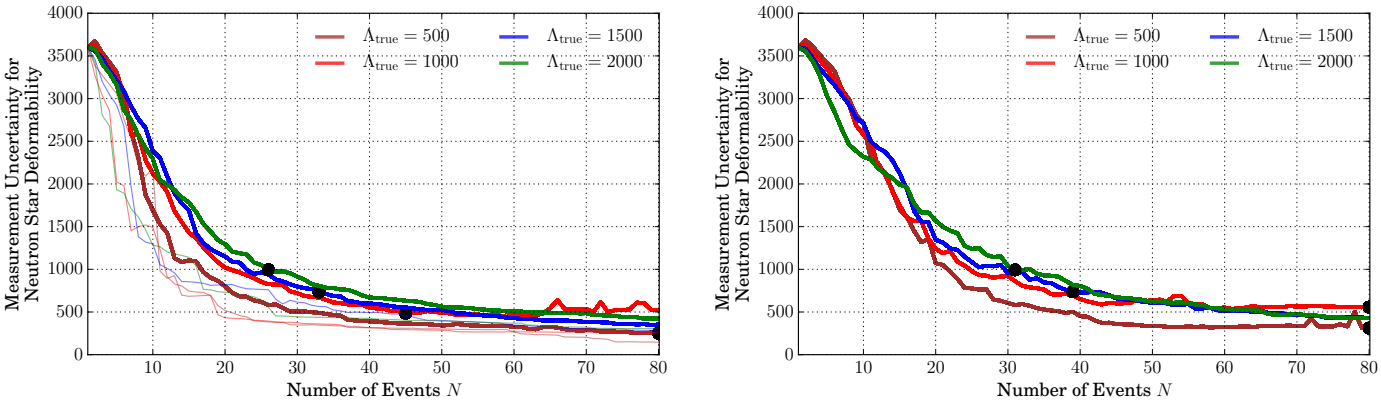

FIG. 11. **No Mass-Gap** (*left*): This panel shows the width of $\Lambda_{\rm NS}$ interval within which the 90% credible intervals for $\Lambda_{\rm NS}$ lie, for 90% of the populations in each ensemble, as a function of the number of observed events N. Details of how this is calculated are given in the text. The populations are sampled under paradigm A, which allows BH masses to fall within the astrophysical mass-gap. Each panel corresponds to a unique value of populations' $\Lambda_{\rm NS}$, decreasing from 2000 → 500 as we go from top to bottom. One curve in each ensemble is highlighted in color (thin lines), representing the realizations already plotted in Fig. 9. **Mass-Gap** (*right*): This panel shows populations drawn under paradigm B, which respects the mass-gap. We find that with approximately 25 or so events, we begin to put statistically meaningful constraints on $\Lambda_{\rm NS}$, restricting it to within ±50% of the true value. We can expect to achieve this with a few years of design aLIGO operation [82]. Further tightening of $\Lambda_{\rm NS}$ credible intervals will require 40+ events.

We restrict ourselves to positive aligned BH spins, since binaries with anti-aligned spins have very little information to add at realistic SNRs, as demonstrated in Fig. 6. This is to be taken into account when the number of observations is related to detector operation time. We repeat this process till we have an ordered set of N events. Since we want to analyze not just a single realization of an astrophysical population, but an ensemble of them, we make an additional approximation to mitigate computational cost. Complete Bayesian parameter estimation is performed for a set of simulated signals whose parameters are the vertices of a regular hyper-cubic grid (henceforth "G") in the space of $\{q\} \times \{\chi_{\rm BH}\} \times \{\rho\}$, with each sampled at $q = \{2, 3, 4, 5\}$, $\chi_{\rm BH} = \{-0.5, 0, 0.5, 0.75\}$, and $\rho = \{10, 20, 30, 50, 70\}$. All events in each population draw are substituted by their respective nearest neighbours on the grid G. Our chosen signal parameter distribution is different from some other studies in literature, which often sample from more astrophysically motivated population distribution functions [99]. We chose one that is sufficiently agnostic in absence of actual known NSBHs, and pragmatic enough for generating population ensembles.

In Fig. 8 we show illustrative results for a single population with neutron star deformability $\Lambda_{\rm NS} = 800$. In the top panel, each curve shows the probability distributions for $\Lambda_{\rm NS}$ as inferred from N events, with N ranging from $1 - 80$. We also mark the 90% credible intervals associated with each of the probability distribution curves. The first few observations do not have enough information to bound $\Lambda_{\rm NS}$ much more than our prior from Eq. 14 does. In the bottom panel, we present information derived from the top panel. The line-circle curve shows the measured median value from N observations. The pair of dashed (dotted) horizontal lines mark ±25% (±50%) error bars. At each N, the range spanned by the filled region is the 90% credible interval deduced from the same events. This figure somewhat quantifies the qualitative deductions we made from the left panel. We find that the median does track the true value quickly, reaching within its 10% with $10 - 15$ observations. This is as one expects of injections in zero noise where random fluctuations are unable to shift the median away from the true value, so long as the measurement is not restricted by the prior. With the same information, our credible intervals also shrink to ±25%. In Fig. 9 we show further results from four independent populations for $\Lambda_{\rm NS} = \{500, 1000, 1500, 2000\}$. As in the right panel of Fig. 8, the line-circle curves track the median $\Lambda_{\rm NS}$, while the filled regions show the associated 90% credible intervals. From the figure, we observe the following: (i) the shrinkage of credible interval widths with increasing N happens in a similar manner for each $\Lambda_{\rm NS}$, and (ii) it takes approximately 20 events to distinguish definitively (with 90% credibility) between deformable NSs with $\Lambda_{\rm NS} = 2000$ and compact NSs with $\Lambda_{\rm NS} = 500$, or equivalently to distinguish between hard, moderate and soft nuclear equations of state. This is comparable to what has been found for binary neutron stars [81, 84, 100].

So far we have discussed individual realizations of NSBH populations. The underlying stochasticity of the population generation process makes it difficult to draw generalized inferences (from a single realization of an NSBH population) about the measurability of $\Lambda_{\rm NS}$. In order to mitigate this, we discuss ensembles of population draws next. In Fig. 10 we show the median $\Lambda_{\rm NS}$ as a func-

tion of the number of observed events, for four population ensembles, with a hundred population draws in each ensemble. Lets focus on the *top left* panel first. In it, we show the median $\Lambda_{\rm NS}$ for all populations in four ensembles, with true $\Lambda_{\rm NS} = \{2000, 1500, 1000, 500\}$ from top to bottom. Populations highlighted in color are simply those that we discussed in Fig. 9. Dash-dotted horizontal lines demarcate $\pm 10\%$ error intervals around the true $\Lambda_{\rm NS}$ values. The panel just below it shows the range of $\Lambda_{\rm NS}$ that encloses the median $\Lambda_{\rm NS}$ for 90% of the populations in *each* ensemble. In other words, this panel shows the range of $\Lambda_{\rm NS}$ within which the median $\Lambda_{\rm NS}$ value for 90% of NSBH populations is expected to lie. From these panels, we observe that our median $\Lambda_{\rm NS}$ values will be within 10% of the *true* value after ~ 25 detections of less deformable neutron stars ($\Lambda_{\rm NS} \leq 1000$), or after as few as 15 detections of more deformable neutron stars ($\Lambda_{\rm NS} \geq 1500$). This is not surprising because we inject simulated signals in *zero* noise, which ensures that the median not be shifted away from the true value. That it takes 15+ events for the median to approach the true value is a manifestation of the fact that the measurement is limited by the prior on $\Lambda_{\rm NS}$ when we have fewer than 15 events. The results discussed in Fig. 8, 9 and the left two panels of Fig. 10 apply to the parameter distribution spanned by the grid G. This distribution allows for $m_{\rm BH}$ as low as $2.7 M_\odot$ (i.e. $q = 2$). Given that disruptive signatures are strongest for small $m_{\rm BH}$, we now investigate an alternate paradigm in which no black hole masses fall within the mass gap $2 - 5 M_\odot$ suggested by astronomical observations [74–77]. We will henceforth denote our standard paradigm, which does not respect the mass-gap, as paradigm A; with paradigm B being this alternate scenario. Both right panels of the figure are identical to their corresponding left panels, but drawn under population paradigm B. Under this paradigm, we expectedly find that information accumulation is much slower. It would take $25 - 40$ detections with $\rho \geq 10$ under this paradigm, for our median $\Lambda_{\rm NS}$ to converge within 10% of its true value.

Finally, we investigate the statistical uncertainties associated with $\Lambda_{\rm NS}$ measurements. We use 90% credible intervals as our measure of the same. First, we draw an ensemble of a hundred populations each for $\Lambda_{\rm NS} = \{500, 1000, 1500, 2000\}$. For each population i in each ensemble, we construct its 90% credible interval $[\Lambda^{90\%}_{{\rm NS}\ i-}, \Lambda^{90\%}_{{\rm NS}\ i+}]$. Next, we construct the interval $[X^-, Y^-]$ that contains $\Lambda^{90\%}_{{\rm NS}\ i-}$ for 90% of the populations in each ensemble; and similarly $[X^+, Y^+]$ for $\Lambda^{90\%}_{{\rm NS}\ i+}$. Finally, in the left panel of Fig. 11, we show the conservative width $|Y^+ - X^-|$ that contains the 90% credible intervals for 90% of all populations in each ensemble [12]. From top to bottom, the population $\Lambda_{\rm NS}$ decreases from $\Lambda_{\rm NS} = 2000 \to 500$, corresponding to decreasingly deformable NSs with softer equations of state. We observe the following: (i) for moderately-hard to hard equations of state with $\Lambda_{\rm NS} \geq 1000$, we can constrain $\Lambda_{\rm NS}$ within $\pm 50\%$ using only $10 - 20$ events, and within $\pm 25\%$ (marked by black circles) with $25 - 40$ events; (ii) for softer equations of state with $\Lambda_{\rm NS} < 1000$, we will achieve the same accuracy with $20 - 30$ and 50+ events, respectively; and (iii) for the first 5 or so observations, our measurement spans the entire prior allowed range: $\Lambda_{\rm NS} \in [0, 4000]$, as shown by the plateauing of the 90% credible intervals towards the left edge to 90% of 4000, i.e. 3600. The right panel in Fig. 11 is identical to the left one, with the difference that populations are drawn under paradigm B, which does *not* allow for BH masses to fall within the mass-gap. We find that for NSs with $\Lambda_{\rm NS} \leq 1000$, it would take $25 - 40$ events to constrain $\Lambda_{\rm NS}$ within $\pm 50\%$ and 50+ events to constrain it within $\pm 25\%$. This is somewhat slower than paradigm A, as is to be expected since here we preclude the lowest mass-ratios, which correspond to signals with largest tidal signatures. For $\Lambda_{\rm NS} > 1000$ we find that we can constrain $\Lambda_{\rm NS}$ within $\pm 50\%$ with a similar number of events as for paradigm A, but will need more ($30 - 40$, as compared to $25 - 40$) events to further constrain it to within $\pm 25\%$ of the true value. Under either paradigms, we find that measuring $\Lambda_{\rm NS}$ better than 25% will require $\mathcal{O}(10^2)$ observations of disruptive NSBH mergers. These results demonstrate that our probed set of disruptive NSBH mergers is as informative of NS tidal properties as are BNS populations, if we assume a uniform mass distribution for NSs and zero NS spins, and possibly more if NS masses are not distributed uniformly [84]. However, being a subset of all NSBH binaries, the accumulation of information from NSBH signals in general may be slower than from binary neutron stars, depending on the distribution of BH masses in coalescing NSBH binaries.

To summarize, in this section we study the improvement in our measurement of NS deformability parameter $\Lambda_{\rm NS}$ with an increasing number of events. We do so by simulating plausible populations of disrupting NSBH binaries (with $\rho \geq 10$). We find that: (i) for more deformable neutron stars (harder equation of states), the median value of $\Lambda_{\rm NS}$ comes within 10% of the true value with as few as 10 events, while achieving the same accuracy for softer equations of state will take $15 - 20$ source detections; (ii) the statistical uncertainty associated with $\Lambda_{\rm NS}$ measurement shrinks to within $\pm 50\%$ with $10 - 20$ events, and to within $\pm 25\%$ with 50+ events, when source $\Lambda_{\rm NS} \geq 1000$; (iii) for softer equations of state, the same could take $25 - 40$ and 50+ events, respectively for the two uncertainty thresholds; and (iv) if BHs really do observe the astrophysical mass-gap, the information accumulation is somewhat slower than if they do not. We conclude that within $20 - 30$ observations, aLIGO would begin to place very interesting bounds on the NS deformability, which would allow us to rule out or rank different equations of state for neutron star matter. Our key findings are summarized in Fig. 10 and 11.

[12] Drawn under paradigm A (mass-gap not respected).

VI. DISCUSSION

The pioneering terrestrial observation of gravitational waves by Advanced LIGO harbingers the dawn of an era of gravitational-wave astronomy where observations would finally drive scientific discovery [101]. As confirmed by the first observations [19, 101, 102], stellar-mass compact binary mergers emit GWs right in the sensitive frequency band of the LIGO observatories, and are their primary targets. Neutron star black hole binaries form a physically distinct sub-class of compact binaries. We expect to detect the first of them in the upcoming observing runs [103], and subsequently at a healthy rate of $0.2 - 300$ mergers a year when aLIGO detectors reach design sensitivity [32].

NSBH binaries are interesting for various reasons. Unlike BBHs, the presence of matter allows for richer phenomena to occur alongside the strong-field gravitational dynamics. The quadrupolar moment of the NS changes during the course of inspiral, which increases the inspiral rate of the binary and alters the form of the emitted gravitational waves. Close to merger, under restricted but plausible conditions, the neutron star is disrupted by the tidal field of its companion black hole and forms an accretion disk around it. This disruption reduces the quadrupolar moment of the system, and decreases the amplitude of the emitted GWs from the time of disruption through to the end of ringdown. Both of these phenomena are discernible in their gravitational-wave signatures alone. In addition, if the neutron star matter is magnetized, the magnetic winding above the remnant black hole poles can build up magnetic fields sufficiently to power short gamma-ray bursts (SGRB) [39, 40, 42–45]. Therefore a coincident observation of gravitational waves from an NSBH merger and a SGRB can potentially confirm the hypothesis that the former is a progenitor of the latter [33–41].

In this paper we study the observability of tidal signatures in the gravitational-wave spectrum of NSBH binaries. More specifically, we investigate three questions. First, what is the effect of not including tidal effects in templates while characterizing NSBH signals? Second, if we do include tidal effects, how well can we measure the tidal deformability of the NS (parameterized by $\Lambda_{\rm NS}$) from individual NSBH signals? And third, as we observe more and more signals, how does our knowledge of $\Lambda_{\rm NS}$ improve? In the following, we summarize our main findings.

First, we study the effects of not including tidal terms in our search templates while characterizing NSBH signals. We expect that the waveform template that best fits the signal would compensate for the reduced number of degrees of freedom in the template model by moving away from the true parameters of the binary. This should result in a *systematic* bias in the recovered values of non-tidal source parameters, such as its masses and spins. In order to quantify it, we inject tidal signals into zero noise, and perform a Bayesian parameter estimation analysis on them using templates *without* tidal terms. We use the LEA+ model (c.f. Sec. II A) to produce tidal waveforms that incorporate the effect of NS distortion during inspiral, and of its disruption close to merger. Our injected signals sample the region of NSBH parameter space where NS disruption prior to binary merger is likely *and* can be modeled using LEA+. Their parameters are given by combinations of $q = m_{\rm BH}/m_{\rm NS} = \{2, 3, 4, 5\}, \chi_{\rm BH} = \{-0.5, 0, 0.5, 0.75\}$ and $\Lambda_{\rm NS} = \{500, 800, 1000, 1500, 2000\}$. Other parameters, such as source location and orientation, that factor out of $h(t)$ as amplitude scaling are co-sampled by varying $\rho = \{20, 30, 50, 70\}$.

At low to moderate SNRs ($\rho \lesssim 30$), we find that using BBH templates does not significantly hamper our estimation of non-tidal parameters for NSBH signals. In the worst case, when the BH mass is within the astrophysical mass-gap [74–77] and its spin is positive aligned, the systematic biases in η and $\chi_{\rm BH}$ measurements do become somewhat comparable to statistical errors (ratio $\sim 0.5 - 0.8$) under very restrictive conditions [13], but never exceed them. At high SNRs ($\rho \gtrsim 50$), systematic biases in $\mathcal{M}_c$ become larger than the statistical uncertainties. For η and $\chi_{\rm BH}$ the difference is more drastic with the systematics reaching up to $4\times$ the statistical errors. We therefore conclude that $\rho \simeq 30 - 50$ is loud enough to motivate the use of tidal templates for even the estimation of non-tidal parameters from NSBH signals. We also conclude that low-latency parameter estimation algorithms, designed to classify GW signals into electromagnetically active (NSBH and NSNS) and inactive (BBH) sources, can use BBH templates to trigger GRB alerts [50, 104–108] for NSBH signals with low to moderate SNRs ($\rho \lesssim 30$). This is so because the primary requirement of identifying NS-X binaries (X = {NS, BH}) can be achieved just as easily with BBH templates, on the basis of the smaller component's mass[14]. We also speculate that NSBH detection searches are unlikely to be affected by the choice of ignoring tidal effects in matched-filtering templates, if these effects are too subtle to manifest in parameter estimation below $\rho \simeq 30$.

Second, we turn the question around to ask: can we measure the tidal effects if our template models did account for them? Tidal effects in our waveform model are parameterized using a single deformability parameter $\Lambda_{\rm NS} \propto (R/M)^5_{\rm NS}$. In order to quantify the measurability of $\Lambda_{\rm NS}$, we inject the same tidal signals as before, and this time perform a Bayesian analysis on them using *tidal* templates. The results are detailed in Sec. IV. At low SNRs ($\rho \simeq 20$), we find that the best we can do is to

[13] requiring a companion BH with mass $m_{\rm BH} \lesssim 4.5 M_\odot$ (i.e. in the astrophysical mass-gap), and the hardest NS EoS considered (with $\Lambda_{\rm NS} \simeq 2000$).

[14] The smaller component mass is unlikely to be significantly biased by missing tidal effects in filter templates below $\rho \simeq 30$, as we show above.

constrain $\Lambda_{\rm NS}$ within $\pm75\%$ of its true value at 90% credible level. This too only if the BH is spinning sufficiently rapidly, with $\chi_{\rm BH} \gtrsim +0.7$, and the NS has $\Lambda_{\rm NS} \gtrsim 1000$. At moderate SNRs ($\rho \simeq 30$), we can constrain $\Lambda_{\rm NS}$ a little better, i.e. within $\pm50\%$ of its true value. This level of accuracy, however, again requires that BH spin $\chi_{\rm BH} \gtrsim +0.7$ and $\Lambda_{\rm NS} \gtrsim 1000$. Binaries with smaller BH spins and/or softer NS EoSs will furnish worse than $\pm75\% - \pm100\%$ errors for $\Lambda_{\rm NS}$. This trend continues as we increase the SNR from $\rho = 30 - 50$. It is not before we reach an SNRs as high as $\rho \simeq 70$ that we can shrink $\Lambda_{\rm NS}$ errors substantially with a single observation (i.e. within $\pm25\%$ of its true value). In summary, we find that with a single but moderately loud NSBH signal, Advanced LIGO can begin to put a factor of $1-2\times$ constraints on NS tidal deformability parameter. These constraints can subsequently be used to assess the likelihood of various candidate equations of state for nuclear matter, and possibly to narrow the range they span.

Third, knowing that single observations can furnish only so much information about the NS equation of state, we move on to investigate how well we do with multiple signals. In order to quantify how $\Lambda_{\rm NS}$ measurement improves with the number of observed events N, we generate populations of NSBH signals and combine the information extracted from each event. The population generation procedure is as follows. The neutron star mass is held fixed at $1.35M_\odot$, its spin at $\chi_{\rm NS} = 0$, and its tidal deformability is fixed to each of $\Lambda_{\rm NS} = \{500, 1000, 1500, 2000\}$. Black hole mass is sampled uniformly from the range $[2,5] \times 1.35 = [2.7, 6.75] M_\odot$, and spin from $\chi_{\rm BH} \in [0,1]$. As before, our parameter choice here is given by the intersection set of the mass range that allows for neutron star disruption and the range supported by LEA+ [45, 65, 109]. In order to keep the computational cost reasonable, we make an additional approximation. For every population generated, we replace the parameters of each event by their nearest neighbor on the uniform grid G, which has vertices at: $q = \{2,3,4,5\} \times \chi_{\rm BH} = \{-0.5, 0, 0.5, 0.75\} \times \Lambda_{\rm NS} = \{500, 800, 1000, 1500, 2000\} \times \rho = \{10, 20, 30, 50, 70\}$. This way, we only have to run full Bayesian parameter estimation analysis on this fixed set of signals. There are two sources of error that enter the deductions we make from a single population generated in the manner described above. First, since the injection parameters are pushed to their nearest neighbor on a grid, we find discrete jumps in $\Lambda_{\rm NS}$ errors as a function of N. And second, an individual population is one particular realization of a stochastic process and could have excursions that may never be found in another population. To account for both of these limitations, we generate an ensemble of populations, and conservatively combine information from all of them[15].

We probe two astrophysical paradigms, one that allows for BH masses to lie within the astrophysical mass-gap (paradigm A), and one that does not (paradigm B). *For paradigm A*, we find the following: (i) for the softer equations of state that result in less deformable neutron stars, $15-20$ detections bring the measured probability distribution for $\Lambda_{\rm NS}$ entirely within the prior, which ensures that the median $\Lambda_{\rm NS}$ tracks the true value to within 10%. (ii) For NSBH populations with more deformable NSs ($\Lambda_{\rm NS} > 1000$), the same is achievable within as few as 10 (or 15 at most) realistic observations. (iii) The statistical uncertainty associated with $\Lambda_{\rm NS}$ measurement can be restricted to be within $\pm50\%$ using $10-20$ observations when $\Lambda_{\rm NS} > 1000$), and using $25-40$ observations for softer equations of state. All of the above is possible within a few years of design aLIGO operation [82], if astrophysical BHs are allowed masses $< 5M_\odot$ (i.e. in the mass-gap). However, further restricting $\Lambda_{\rm NS}$ will require 50+ NSBH observations. *For paradigm B*, we find the information accumulation to be somewhat slower. While the quantitative inferences for populations with $\Lambda_{\rm NS} > 1000$ are not affected significantly, we find that $\Lambda_{\rm NS} < 1000$ populations require $10-20\%$ more events to attain the same measurement accuracy as under paradigm A. In either case, the accumulation of information from the general NSBH population will likely be slower than from BNS inspirals [60, 61, 84, 99], depending on the mass distribution of stellar-mass black holes. Though, template models for the latter may be more uncertain due to missing point-particle PN terms at orders comparable to tidal terms [60]. We conclude that within as few as $20-30$ observations of disruptive NSBH mergers, aLIGO will begin to place interesting bounds on NS deformability. This, amongst other things, will allow us to rank different equations of state for neutron star matter from most to least likely, within a few years' detector operation. Our methods and results are detailed in Sec. V.

Finally, we note that the underlying numerical simulations used to calibrate the waveform model used here have not been verified against independent codes so far. It is therefore difficult to assess the combined modeling error of LEA+ and its effect on our results. Our results here are, therefore, limited by the limitations of our waveform model, and presented with this caveat. However, we do expect the combined effect of modeling errors to *not* affect our *qualitative* conclusions, especially since the underlying point-particle component of LEA+ includes all high-order terms, unlike past BNS studies [60, 61] In future, we plan to further the results presented here by using more recent tidal models [83, 110], that may improve upon LEA+[16].

[15] See Sec. V for further details.

[16] One of them [83] is only an amplitude model though, which has to be augmented with a compatible phase model first.

ACKNOWLEDGMENTS

We thank Benjamin Lackey, Francesco Pannarale, Francois Foucart, and Duncan Brown for helpful discussions. We gratefully acknowledge support for this research at CITA from NSERC of Canada, the Ontario Early Researcher Awards Program, the Canada Research Chairs Program, and the Canadian Institute for Advanced Research. Calculations were performed at the Vulcan supercomputer at the Albert Einstein Institute; H.P. and P.K. thank the Albert-Einstein Institute, Potsdam, for hospitality during part of the time where this research was completed. M.P. thanks CITA for hospitality where part of the work was carried out.

Appendix A: Statistical uncertainty in measuring non-tidal parameters

In Fig. 12, we show how *precisely* can we measure non-tidal NSBH parameters $X = \{\mathcal{M}_c, \eta, \chi_{\rm BH}\}$ using BBH templates. The three panels correspond to $\mathcal{M}_c$ (top), η (middle), and $\chi_{\rm BH}$ (bottom), and show the width of these credible intervals $(\Delta X)^{90\%}$ as a function of BH mass/spin (within each sub-panel), and NS properties, i.e. $\Lambda_{\rm NS}$ (downwards in each column) [17]. From the left-most column, we find that: (i) at $\rho = 20$ the chirp mass is measured remarkably well - to a precision of 0.16% of its true value, and (ii) so is $\chi_{\rm BH}$. (iii) The dimensionless mass-ratio η is determined more loosely, with $25+\%$ uncertainty. If the signal is even louder ($\rho \geq 30$), all three measurements gain further precision, especially η, for which the relative errors shrink down to single-digit percents. We remind ourselves that these results do not tell the full story since the precision of a measurement is only meaningful if the measurement is accurate to begin with. In our case there are tidal effects that have not been incorporated into our search (BBH) templates, which can lead to a systematic bias in parameter recovery. We refer the reader to Sec. III for a comparative study of both systematic and statistical errors.

Appendix B: Illustrations of Bayesian posteriors

In Fig. 13 we show the correlation of mass, spin, and tidal parameter measurements. We keep the binary parameters as in Fig. 5, with $\Lambda_{\rm NS} = 2000$, and set $\rho = 20$ (left panel) or $\rho = 50$ (right panel). We find that the measurement of $\Lambda_{\rm NS}$ is weakly degenerate with other parameters, and at realistic SNRs it would improve by a few tens of percent if we knew non-tidal parameters to better accuracy. The predominant factor that would enhance the measurement accuracy for $\Lambda_{\rm NS}$ is nevertheless the signal strength. Only when $\rho \gtrsim 50$ can we expect $\Lambda_{\rm NS}$ measurement to be limited by its degeneracy with non-tidal parameters (at a factor of few level), as also reported by previous studies [65].

Appendix C: Phenomenology of $\Lambda_{\rm NS}$ measurement errors

Here, we quantitatively explore the dependence of our statistical uncertainties for $\Lambda_{\rm NS}$ on the number of events, as well as on the true NS deformability itself. First, we will focus on the dependence on N. We assume a power-law dependence of the form $\delta\Lambda_{\rm NS} \propto 1/N^{\alpha}$. For each of the 100 populations for each of $\Lambda_{\rm NS} = 500 - 2000$, we compute the exponent α as a function of the number of observed events N, and show it in Fig. 14. There are $100 \times 5 = 500$ curves on the figure, with one highlighted for each value of population's $\Lambda_{\rm NS}$. These highlighted values are only special in the sense that they correspond to populations discussed earlier in this section (c.f. Fig. 8-9). We immediately observe two things, (i) there is a globally similar dependence on N for all populations, and (ii) information accumulates *faster* than $1/\sqrt{N}$. In fact, we find that if $\delta\Lambda_{\rm NS} \propto \frac{1}{N^{\alpha}}$, α lines in the range $0.7^{+0.2}_{-0.2}$. Next, we focus on the dependence of $\delta\Lambda_{\rm NS}$ on $\Lambda_{\rm NS}$ of the population itself. As suggested by Fisher-matrix studies [65], and as for N, we assume the form $\delta\Lambda_{\rm NS} \propto \Lambda^{\beta}_{\rm NS}$. From each set of 100 populations with a given $\Lambda_{\rm NS}$ value, we draw one at random, and form a set of 5 similarly drawn populations, one for each of $\Lambda_{\rm NS} = \{500, 800, 1000, 1500, 2000\}$. With each set, we determine β for different number of observed events N. In all, we make 100 independent 5−population sets and show the value of β measured from each in Fig. 15. We find that the assumed relation $\delta\Lambda_{\rm NS} \propto \Lambda^{\beta}_{\rm NS}$ gets fairly robust for larger values of N, with β converging to $\beta = 0.5^{+0.33}_{-0.33}$. The fact that $0 < \beta < 1$ implies that the relative error $\delta\Lambda_{\rm NS}/\Lambda_{\rm NS}$ *decreases* with increasing $\Lambda_{\rm NS}$, while the absolute error *increases*. From these results, we conclude that the measurement uncertainty for $\Lambda_{\rm NS}$ after N observations is

$$\delta\Lambda_{\rm NS} \propto \frac{\Lambda_{\rm NS}^{0.5^{+0.33}_{-0.33}}}{N^{0.7^{+0.2}_{-0.2}}}. \tag{C1}$$

We also find that while these results are inferred from paradigm A populations, paradigm B gives very similar results.

REFERENCES

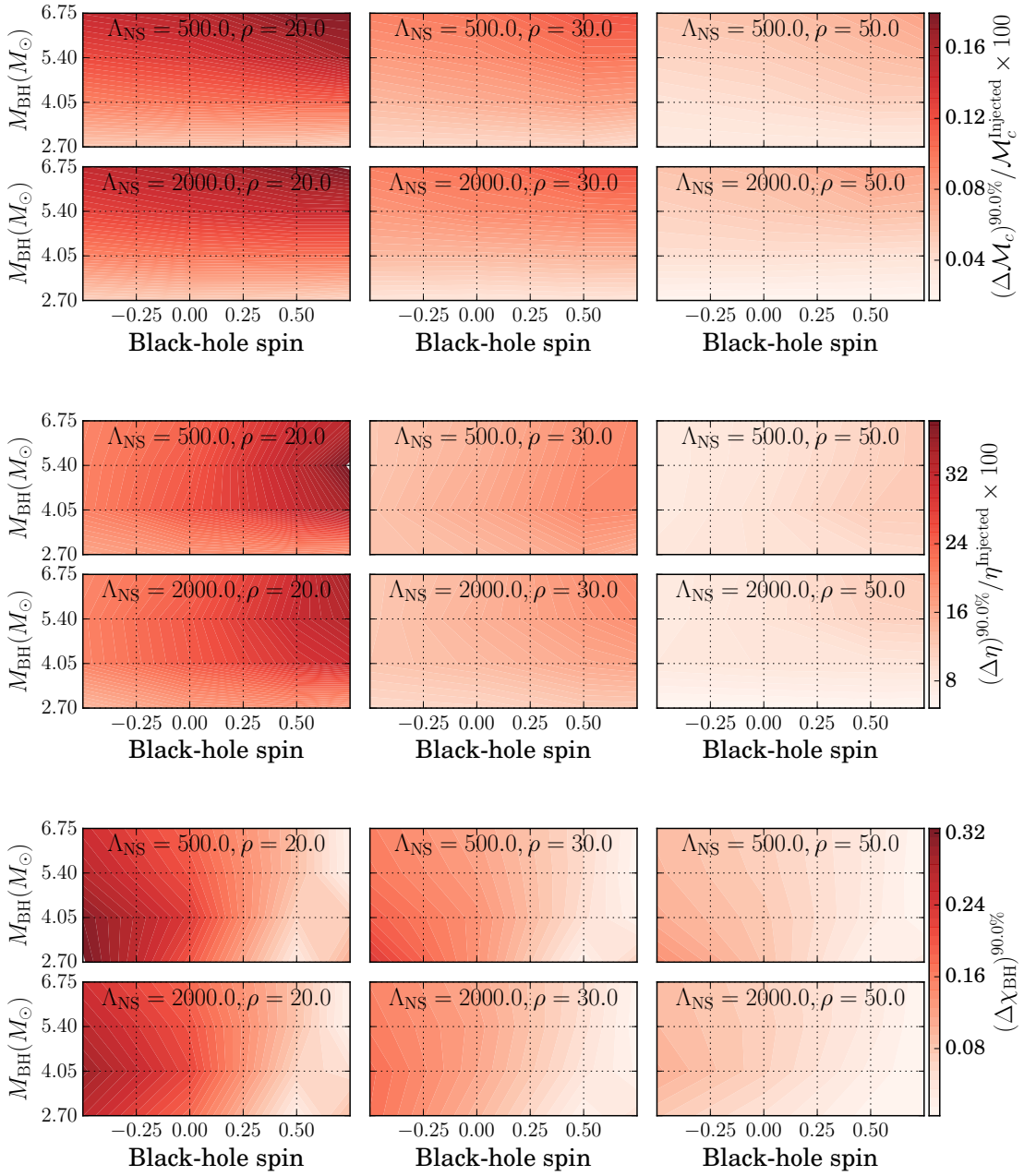

FIG. 12. **Statistical measurement uncertainty for NSBH parameters, ignoring tidal effects:** We show here the statistical uncertainty associated with our measurement of non-tidal parameters $\mathcal{M}_c, \eta$, and $\chi_{\rm BH}$ (at 90% credibility), over the signal parameter space. Individual panels show the same as a function of BH mass and spin. Across each row, we see the effect of increasing signal strength (i.e. SNR) with the tidal deformability of the NS $\Lambda_{\rm NS}$ fixed. Down each column, we see the effect of increasing $\Lambda_{\rm NS}$, at fixed SNR. Tidal effects are ignored in templates.

[17] We restrict NS mass to $1.35M_\odot$ and its spin to zero. Varying its tidal deformability $\Lambda_{\rm NS}$ does not significantly change the measurement uncertainties for non-tidal binary parameters, as is evident from comparing the two rows in each panel of Fig. 12.

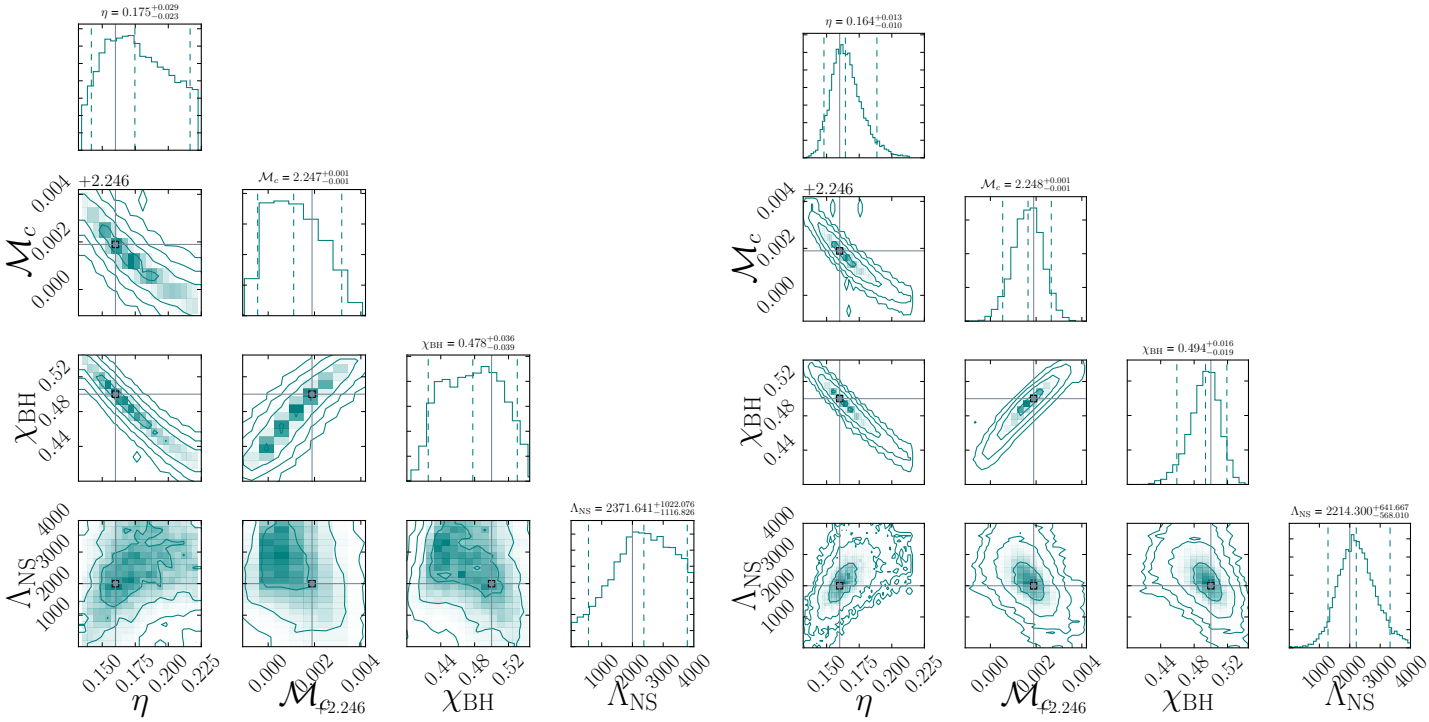

FIG. 13. **Illustrative posterior probability distributions for NSBH parameters, for signals at different SNRs:** We illustrate here two sets of two-dimensional joint probability distributions, differing only in signal strength, with $\rho = 20$ in the left panel, and $\rho = 50$ in the right. The injected parameters are $q = m_{\rm BH}/m_{\rm NS} = 5.4M_\odot/1.35M_\odot = 4$, $\chi_{\rm BH} = +0.5$, and $\Lambda_{\rm NS} = 2000$. Contours are shown for $\{1-, 2-, 3-, \cdots\}\sigma$ confidence levels. Templates include tidal effects, as evident in the bottom rows of both panels which show the correlation of $\Lambda_{\rm NS}$ with non-tidal parameters. Contrasting the two panels illustrates the effect of increasing the SNR on various parameter measurements.

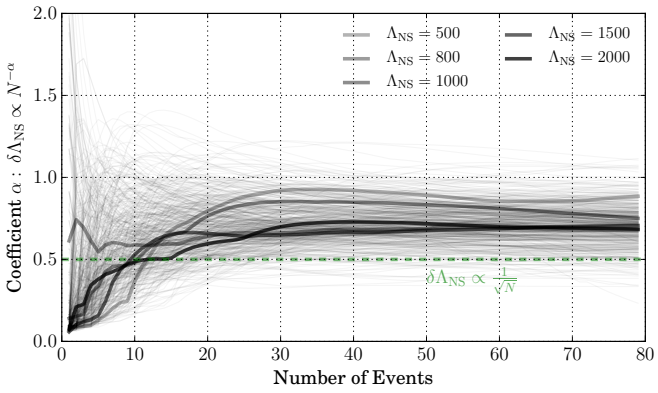

FIG. 14. Assuming a power-law dependence of the measurement error on the number of events: $\delta\Lambda_{\rm NS} \propto 1/N^\alpha$, we show α in this figure as a function of the number of observed events N. Shown are five families of 100 population draws each, with each family corresponding to one of $\Lambda_{\rm NS} = \{500, 800, 1000, 1500, 2000\}$. Each grey curve corresponds to one of these $100 \times 5 = 500$ populations. The thicker curves, one from each family, shows the population we discussed in Fig. 8-9. We find that a power-law is a good approximation for the concerned dependence, and information accumulates *faster* than $1/\sqrt{N}$. We estimate $\alpha \simeq 0.7^{+0.2}_{-0.2}$.

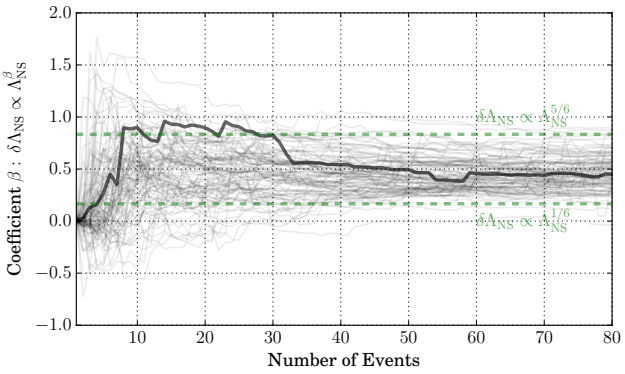

FIG. 15. In this figure, which is similar to Fig. 14, we quantify the dependence of $\delta\Lambda_{\rm NS}$ on $\Lambda_{\rm NS}$ itself. Of the five families of simulated NSBH populations, we construct 100 independent sets taking one population from each family. With each of these 100 sets, and assuming a power-law dependence: $\delta\Lambda_{\rm NS} \propto \Lambda_{\rm NS}^{\beta}$, we estimate β and show it in this figure as a function of the number of observed events N. The thicker curve corresponds to the populations discussed in Fig. 9. We find that β can be estimated to lie within $[1/6, 5/6]$ with a likely value close to $1/2$. Since $0 < \beta < 1$, the relative error $\delta\Lambda_{\rm NS}/\Lambda_{\rm NS}$ *decreases* as the star gets more deformable, while the absolute error $\delta\Lambda_{\rm NS}$ *increases*.

[1] D. Shoemaker (LIGO Collaboration), "Advanced LIGO anticipated sensitivity curves," (2010), LIGO Document T0900288-v3.

[2] B. P. Abbott *et al.* (LIGO Scientific Collaboration, Virgo Collaboration), Phys. Rev. Lett. **116**, 061102 (2016), arXiv:1602.03837 [gr-qc].

[3] The Virgo Collaboration, "Advanced Virgo Baseline Design," (2009), [VIR-0027A-09].

[4] F. Acernese *et al.* (Virgo Collaboration), Class. Quantum Grav. **32**, 024001 (2015), arXiv:1408.3978 [gr-qc].

[5] Y. Aso, Y. Michimura, K. Somiya, M. Ando, O. Miyakawa, T. Sekiguchi, D. Tatsumi, and H. Yamamoto (The KAGRA Collaboration), Phys. Rev. D **88**, 043007 (2013), arXiv:1306.6747 [gr-qc].

[6] K. Somiya (KAGRA Collaboration), Class. Quantum Grav. **29**, 124007 (2012), arXiv:1111.7185 [gr-qc].

[7] C. S. Unnikrishnan, International Journal of Modern Physics D **22**, 1341010 (2013).

[8] F. X. Timmes, S. E. Woosley, and T. A. Weaver, Astrophys. J. **457**, 834 (1996), arXiv:astro-ph/9510136 [astro-ph].

[9] C. L. Fryer, Astrophys. J. **522**, 413 (1999), arXiv:astro-ph/9902315 [astro-ph].

[10] S. E. Woosley, A. Heger, and T. A. Weaver, Rev. Mod. Phys. **74**, 1015 (2002).

[11] K. Belczynski, T. Bulik, C. L. Fryer, A. Ruiter, F. Valsecchi, J. S. Vink, and J. R. Hurley, apj **714**, 1217 (2010), arXiv:0904.2784 [astro-ph.SR].

[12] K. Belczynski, M. Dominik, T. Bulik, R. O'Shaughnessy, C. Fryer, and D. E. Holz, Astrophys. J. Lett. **715**, L138 (2010), arXiv:1004.0386 [astro-ph.HE].

[13] M. Dominik, E. Berti, R. O'Shaughnessy, I. Mandel, K. Belczynski, C. Fryer, D. Holz, T. Bulik, and F. Pannarale, Astrophys. J. **806**, 263 (2015), arXiv:1405.7016 [astro-ph.HE].

[14] K. Belczynski, V. Kalogera, F. A. Rasio, R. E. Taam, and T. Bulik, Astrophys.J. **662**, 504 (2007), arXiv:astro-ph/0612032 [astro-ph].

[15] C. L. Fryer, K. Belczynski, G. Wiktorowicz, M. Dominik, V. Kalogera, and D. E. Holz, Astrophys. J. **749**, 91 (2012), arXiv:1110.1726 [astro-ph.SR].

[16] N. Wex and S. Kopeikin, Astrophys. J. **514**, 388 (1999), arXiv:astro-ph/9811052 [astro-ph].

[17] R. Narayan, T. Piran, and A. Shemi, Astrophys. J. **379**, L17 (1991).

[18] I. Mandel, C.-J. Haster, M. Dominik, and K. Belczynsk, (2015), 10.1093/mnrasl/slv054, arXiv:1503.03172 [astro-ph.HE].

[19] B. P. Abbott *et al.* (Virgo, LIGO Scientific), (2016), arXiv:1602.03842 [astro-ph.HE].

[20] D. Psaltis, M. van der Klis, T. Strohmayer, L. Bildsten, J. McClintock, R. Remillard, P. Charles, M. Coe, J. Heise, J. in 't Zand, V. Kaspi, M. Roberts, A. Harding, F. Verbunt, W. Lewin, R. Fender, E. Kuulkers, A. Norton, A. Schwope, B. Warner, P. Kahabka, E. van den Heuvel, G. Fabbiano, N. White, A. King, P. Woods, C. Thompson, K. Hurley, R. Sari, S. Djorgovski, and T. Tauris, in *Compact Stellar X-ray Sources*, edited by M. v. d. K. Walter Lewin (Cambridge University Press, 2010) p. 708.

[21] R. A. Remillard and J. E. McClintock, Ann. Rev. As-

tron. Astrophys. **44**, 49 (2006), arXiv:astro-ph/0606352 [astro-ph].
[22] T. Fragos, M. Tremmel, E. Rantsiou, and K. Belczynski, (2010), arXiv:1001.1107 [astro-ph.HE].
[23] R. N. Manchester, G. B. Hobbs, A. Teoh, and M. Hobbs, Astron. J. **129**, 1993 (2005), arXiv:astro-ph/0412641 [astro-ph].
[24] J. M. Lattimer, Ann.Rev.Nucl.Part.Sci. **62**, 485 (2012), arXiv:1305.3510 [nucl-th].
[25] B. Margon, M. Lampton, S. Bowyer, and R. Cruddace, Astrophys. J. Lett. **169**, L23 (1971).
[26] H. E. Bond, R. L. White, R. H. Becker, and M. S. O'Brien, Publ. Astron. Soc. Pac. **114**, 1359 (2002), arXiv:astro-ph/0208383 [astro-ph].
[27] R. A. Hulse and J. H. Taylor, Astrophys. J. **195**, L51 (1975).
[28] J. H. Taylor and J. M. Weisberg, Astrophys. J. **253**, 908 (1982).
[29] J. Weisberg, D. Nice, and J. Taylor, Astrophys.J. **722**, 1030 (2010), arXiv:1011.0718 [astro-ph.GA].
[30] H.-T. Janka, T. Eberl, M. Ruffert, and C. L. Fryer, Astrophys. J. **527**, L39 (1999), astro-ph/9908290.
[31] C. L. Fryer, F. G. Oliveira, J. A. Rueda, and R. Ruffini, Phys. Rev. Lett. **115**, 231102 (2015), arXiv:1505.02809 [astro-ph.HE].
[32] J. Abadie, B. P. Abbott, R. Abbott, M. Abernathy, T. Accadia, F. Acernese, C. Adams, R. Adhikari, P. Ajith, B. Allen, and et al. (LIGO Scientific Collaboration, Virgo Collaboration), Class. Quantum Grav. **27**, 173001 (2010), arXiv:1003.2480 [astro-ph.HE].
[33] D. Eichler, M. Livio, T. Piran, and D. N. Schramm, Nature **340**, 126 (1989).
[34] R. Narayan, B. Paczynski, and T. Piran, Astrophys. J. Lett. **395**, L83 (1992), astro-ph/9204001.
[35] R. Mochkovitch, M. Hernanz, J. Isern, and X. Martin, Nature **361**, 236 (1993).
[36] S. D. Barthelmy *et al.*, Nature **438**, 994 (2005), arXiv:astro-ph/0511579 [astro-ph].
[37] D. B. Fox, D. A. Frail, P. A. Price, S. R. Kulkarni, E. Berger, T. Piran, A. M. Soderberg, S. B. Cenko, P. B. Cameron, A. Gal-Yam, M. M. Kasliwal, D.-S. Moon, F. A. Harrison, E. Nakar, B. P. Schmidt, B. Penprase, R. A. Chevalier, P. Kumar, K. Roth, D. Watson, B. L. Lee, S. Shectman, M. M. Phillips, M. Roth, P. J. McCarthy, M. Rauch, L. Cowie, B. A. Peterson, J. Rich, N. Kawai, K. Aoki, G. Kosugi, T. Totani, H.-S. Park, A. MacFadyen, and K. C. Hurley, Nature **437**, 845 (2005), astro-ph/0510110.
[38] N. Gehrels, C. L. Sarazin, P. T. O'Brien, B. Zhang, L. Barbier, S. D. Barthelmy, A. Blustin, D. N. Burrows, J. Cannizzo, J. R. Cummings, M. Goad, S. T. Holland, C. P. Hurkett, J. A. Kennea, A. Levan, C. B. Markwardt, K. O. Mason, P. Meszaros, M. Page, D. M. Palmer, E. Rol, T. Sakamoto, R. Willingale, L. Angelini, A. Beardmore, P. T. Boyd, A. Breeveld, S. Campana, M. M. Chester, G. Chincarini, L. R. Cominsky, G. Cusumano, M. de Pasquale, E. E. Fenimore, P. Giommi, C. Gronwall, D. Grupe, J. E. Hill, D. Hinshaw, J. Hjorth, D. Hullinger, K. C. Hurley, S. Klose, S. Kobayashi, C. Kouveliotou, H. A. Krimm, V. Mangano, F. E. Marshall, K. McGowan, A. Moretti, R. F. Mushotzky, K. Nakazawa, J. P. Norris, J. A. Nousek, J. P. Osborne, K. Page, A. M. Parsons, S. Patel, M. Perri, T. Poole, P. Romano, P. W. A. Roming, S. Rosen, G. Sato, P. Schady, A. P. Smale, J. Sollerman, R. Starling, M. Still, M. Suzuki, G. Tagliaferri, T. Takahashi, M. Tashiro, J. Tueller, A. A. Wells, N. E. White, and R. A. M. J. Wijers, Nature **437**, 851 (2005), astro-ph/0505630.
[39] M. Shibata, M. D. Duez, Y. T. Liu, S. L. Shapiro, and B. C. Stephens, Phys. Rev. Lett. **96**, 031102 (2006), arXiv:astro-ph/0511142 [astro-ph].
[40] V. Paschalidis, M. Ruiz, and S. L. Shapiro, Astrophys. J. **806**, L14 (2015), arXiv:1410.7392 [astro-ph.HE].
[41] N. R. Tanvir, A. J. Levan, A. S. Fruchter, J. Hjorth, R. A. Hounsell, K. Wiersema, and R. L. Tunnicliffe, Nature **500**, 547 (2013), arXiv:1306.4971 [astro-ph.HE].
[42] F. Foucart, E. O'Connor, L. Roberts, M. D. Duez, R. Haas, L. E. Kidder, C. D. Ott, H. P. Pfeiffer, M. A. Scheel, and B. Szilagyi, Phys. Rev. D **91**, 124021 (2015), arXiv:1502.04146 [astro-ph.HE].
[43] G. Lovelace, M. D. Duez, F. Foucart, L. E. Kidder, H. P. Pfeiffer, M. A. Scheel, and B. Szilágyi, Class. Quantum Grav. **30**, 135004 (2013), arXiv:1302.6297 [gr-qc].
[44] M. B. Deaton, M. D. Duez, F. Foucart, E. O'Connor, C. D. Ott, L. E. Kidder, C. D. Muhlberger, M. A. Scheel, and B. Szilagyi, Astrophys. J. **776**, 47 (2013), arXiv:1304.3384 [astro-ph.HE].
[45] F. Foucart, Phys. Rev. D **86**, 124007 (2012), arXiv:1207.6304 [astro-ph.HE].
[46] F. Foucart, L. Buchman, M. D. Duez, M. Grudich, L. E. Kidder, I. MacDonald, A. Mroue, H. P. Pfeiffer, M. A. Scheel, and B. Szilagyi, Phys. Rev. D **88**, 064017 (2013), arXiv:1307.7685 [gr-qc].
[47] M. Shibata and K. Taniguchi, Phys. Rev. **D77**, 084015 (2008), arXiv:0711.1410 [gr-qc].
[48] V. Ferrari, L. Gualtieri, and F. Pannarale, Phys. Rev. D **81**, 064026 (2010), arXiv:0912.3692 [gr-qc].
[49] K. Kawaguchi, K. Kyutoku, H. Nakano, H. Okawa, M. Shibata, and K. Taniguchi, Phys. Rev. D **92**, 024014 (2015), arXiv:1506.05473 [astro-ph.HE].
[50] B. P. Abbott *et al.* (LIGO Scientific Collaboration, Virgo Collaboration), Living Rev. Rel. **19** (2016), 10.1007/lrr-2016-1, arXiv:1304.0670v3 [gr-qc].
[51] W. H. Lee and W. L. Kluzniak, Astroph. J. **526**, 178 (1999).
[52] W. H. Lee and W. L. Kluzniak, Mon. Not. Roy. Astr. Soc. **308**, 780 (1999).
[53] W. H. Lee, Mon. Not. Roy. Astr. Soc. **318**, 606 (2000).
[54] R. Oechslin, H. T. Janka, and A. Marek, Astron. Astrophys. **467**, 395 (2007), arXiv:astro-ph/0611047.
[55] J. S. Read, B. D. Lackey, B. J. Owen, and J. L. Friedman, Phys. Rev. **D79**, 124032 (2009), arXiv:0812.2163 [astro-ph].
[56] C. Markakis, J. S. Read, M. Shibata, K. Uryu, J. D. E. Creighton, and J. L. Friedman, in *On recent developments in theoretical and experimental general relativity, astrophysics and relativistic field theories. Proceedings, 12th Marcel Grossmann Meeting on General Relativity, Paris, France, July 12-18, 2009. Vol. 1-3* (2010) pp. 743–745, arXiv:1008.1822 [gr-qc].
[57] C. Markakis, J. S. Read, M. Shibata, K. Uryu, J. D. Creighton, *et al.*, J. Phys. Conf. Ser. **189**, 012024 (2009), arXiv:1110.3759 [gr-qc].
[58] N. Stergioulas, A. Bauswein, K. Zagkouris, and H.-T. Janka, Mon. Not. Roy. Astr. Soc. **418**, 427 (2011), arXiv:1105.0368 [gr-qc].
[59] W. E. East, F. Pretorius, and B. C. Stephens, Phys.

Rev. D **85**, 124009 (2012), arXiv:1111.3055 [astro-ph.HE].
[60] B. D. Lackey and L. Wade, Phys. Rev. D **91**, 043002 (2015), arXiv:1410.8866 [gr-qc].
[61] L. Wade, J. D. E. Creighton, E. Ochsner, B. D. Lackey, B. F. Farr, *et al.*, Phys. Rev. D **89**, 103012 (2014), arXiv:1402.5156 [gr-qc].
[62] A. Bauswein, N. Stergioulas, and H.-T. Janka, Phys. Rev. D **90**, 023002 (2014), arXiv:1403.5301 [astro-ph.SR].
[63] É. É. Flanagan and T. Hinderer, Phys. Rev. D **77**, 021502 (2008), arXiv:0709.1915.
[64] K. Kyutoku, M. Shibata, and K. Taniguchi, Phys. Rev. D **82**, 044049 (2010), arXiv:1008.1460 [astro-ph.HE].
[65] B. D. Lackey, K. Kyutoku, M. Shibata, P. R. Brady, and J. L. Friedman, Phys. Rev. D **89**, 043009 (2014), arXiv:1303.6298 [gr-qc].
[66] F. Pannarale, E. Berti, K. Kyutoku, B. D. Lackey, and M. Shibata, (2015), arXiv:1509.06209 [gr-qc].
[67] F. Foucart, M. B. Deaton, M. D. Duez, E. O'Connor, C. D. Ott, R. Haas, L. E. Kidder, H. P. Pfeiffer, M. A. Scheel, and B. Szilagyi, Phys. Rev. D **90**, 024026 (2014), arXiv:1405.1121 [astro-ph.HE].
[68] J. Vines, É. É. Flanagan, and T. Hinderer, Phys. Rev. D **83**, 084051 (2011), arXiv:1101.1673 [gr-qc].
[69] A. Maselli, L. Gualtieri, and V. Ferrari, Phys. Rev. D **88**, 104040 (2013), arXiv:1310.5381 [gr-qc].
[70] K. Barkett, M. A. Scheel, R. Haas, C. D. Ott, S. Bernuzzi, D. A. Brown, B. Szilágyi, J. D. Kaplan, J. Lippuner, C. D. Muhlberger, F. Foucart, and M. D. Duez, Phys. Rev. D **93**, 044064 (2016), arXiv:1509.05782 [gr-qc].
[71] K. Yagi and N. Yunes, Phys. Rev. D **89**, 021303 (2014), arXiv:1310.8358 [gr-qc].
[72] B. D. Lackey, K. Kyutoku, M. Shibata, P. R. Brady, and J. L. Friedman, Phys. Rev. D **85**, 044061 (2012), arXiv:1109.3402 [astro-ph.HE].
[73] M. Vallisneri, Phys. Rev. **D77**, 042001 (2008), arXiv:gr-qc/0703086 [GR-QC].
[74] C. D. Bailyn, R. K. Jain, P. Coppi, and J. A. Orosz, Astrophys. J. **499**, 367 (1998), arXiv:astro-ph/9708032 [astro-ph].
[75] V. Kalogera and G. Baym, Astrophys. J. **470**, L61 (1996), arXiv:astro-ph/9608059 [astro-ph].
[76] L. Kreidberg, C. D. Bailyn, W. M. Farr, and V. Kalogera, Astroph.J. **757**, 36 (2012), arXiv:1205.1805 [astro-ph.HE].
[77] T. B. Littenberg, B. Farr, S. Coughlin, V. Kalogera, and D. E. Holz, (2015), arXiv:1503.03179 [astro-ph.HE].
[78] R. C. Tolman, Phys. Rev. **55**, 364 (1939).
[79] J. R. Oppenheimer and G. M. Volkoff, Phys. Rev. **55**, 374 (1939).
[80] R. C. Tolman, Proceedings of the National Academy of Science **20**, 169 (1934).
[81] W. Del Pozzo, T. G. F. Li, M. Agathos, C. Van Den Broeck, and S. Vitale, Phys. Rev. Lett. **111**, 071101 (2013), arXiv:1307.8338 [gr-qc].
[82] J. Abadie *et al.* (LIGO Scientific Collaboration), Class. Quantum Grav. **27**, 173001 (2010), arXiv:1003.2480 [gr-qc].
[83] F. Pannarale, E. Berti, K. Kyutoku, B. D. Lackey, and M. Shibata, Phys. Rev. D **92**, 084050 (2015), arXiv:1509.00512 [gr-qc].
[84] M. Agathos, J. Meidan, W. D. Pozzo, T. G. F. Li, M. Tompitak, J. Veitch, S. Vitale, and C. V. D. Broeck, Phys. Rev. D **92**, 023012 (2015), arXiv:1503.05405 [gr-qc].
[85] A. Taracchini, Y. Pan, A. Buonanno, E. Barausse, M. Boyle, T. Chu, G. Lovelace, H. P. Pfeiffer, and M. A. Scheel, Phys. Rev. D **86**, 024011 (2012), arXiv:1202.0790 [gr-qc].
[86] A. Buonanno and T. Damour, Phys. Rev. D **59**, 084006 (1999), arXiv:gr-qc/9811091 [gr-qc].
[87] A. Taracchini, A. Buonanno, Y. Pan, T. Hinderer, M. Boyle, D. A. Hemberger, L. E. Kidder, G. Lovelace, A. H. Mroue, H. P. Pfeiffer, M. A. Scheel, B. Szilagyi, N. W. Taylor, and A. Zenginoglu, Phys. Rev. D **89 (R)**, 061502 (2014), arXiv:1311.2544 [gr-qc].
[88] M. Pürrer, (2015), arXiv:1512.02248 [gr-qc].
[89] P. Kumar, K. Barkett, S. Bhagwat, N. Afshari, D. A. Brown, G. Lovelace, M. A. Scheel, and B. Szilágyi, Phys. Rev. D **92**, 102001 (2015), arXiv:1507.00103 [gr-qc].
[90] P. Kumar, T. Chu, H. Fong, H. P. Pfeiffer, M. Boyle, D. A. Hemberger, L. E. Kidder, M. A. Scheel, and B. Szilagyi, Phys. Rev. **D93**, 104050 (2016), arXiv:1601.05396 [gr-qc].
[91] L. S. Collaboration, "LSC Algorithm Library software packages LAL, LALWRAPPER, and LALAPPS," .
[92] M. Pürrer, M. Hannam, and F. Ohme, (2015), arXiv:1512.04955 [gr-qc].
[93] D. Foreman-Mackey, D. W. Hogg, D. Lang, and J. Goodman, arXiv **125**, 306 (2013), arXiv:1202.3665 [astro-ph.IM].
[94] A. Gelman and D. B. Rubin, Statist. Sci. **7**, 457 (1992).
[95] M. Puerrer *et al.*, (2016), in preparation.
[96] B. S. Sathyaprakash and B. F. Schutz, Living Rev. Rel. **12**, 2 (2009), arXiv:0903.0338 [gr-qc].
[97] F. Foucart, M. D. Duez, L. E. Kidder, M. A. Scheel, B. Szilágyi, and S. A. Teukolsky, Phys. Rev. D **85**, 044015 (2012), arXiv:1111.1677 [gr-qc].
[98] B. Kiziltan, A. Kottas, M. De Yoreo, and S. E. Thorsett, Astrophys. J. **778**, 66 (2013).
[99] I. Mandel, Phys. Rev. **D81**, 084029 (2010), arXiv:0912.5531 [astro-ph.HE].
[100] K. Chatziioannou, K. Yagi, A. Klein, N. Cornish, and N. Yunes, Phys. Rev. D **92**, 104008 (2015), arXiv:1508.02062 [gr-qc].
[101] B. P. Abbott *et al.* (Virgo, LIGO Scientific), Phys. Rev. Lett. **116**, 061102 (2016), arXiv:1602.03837 [gr-qc].
[102] B. P. Abbott *et al.* (Virgo, LIGO Scientific), Phys. Rev. Lett. **116**, 241103 (2016), arXiv:1606.04855 [gr-qc].
[103] B. P. Abbott *et al.* (Virgo, LIGO Scientific), (2016), arXiv:1607.07456 [astro-ph.HE].
[104] J. Abadie, B. P. Abbott, R. Abbott, T. D. Abbott, M. Abernathy, T. Accadia, F. Acernese, C. Adams, R. Adhikari, C. Affeldt, and et al., Astron. Astrophys. **541**, A155 (2012), arXiv:1112.6005.
[105] L. P. Singer *et al.*, Astrophys. J. **795**, 105 (2014), arXiv:1404.5623 [astro-ph.HE].
[106] L. P. Singer and L. R. Price, Phys. Rev. **D93**, 024013 (2016), arXiv:1508.03634 [gr-qc].
[107] C. Pankow, P. Brady, E. Ochsner, and R. O'Shaughnessy, Phys. Rev. **D92**, 023002 (2015), arXiv:1502.04370 [gr-qc].
[108] B. P. Abbott *et al.* (InterPlanetary Network, DES, IN-

TEGRAL, La Silla-QUEST Survey, MWA, Fermi-LAT, J-GEM, DEC, GRAWITA, Pi of the Sky, Fermi GBM, MASTER, Swift, iPTF, VISTA, ASKAP, SkyMapper, PESSTO, TOROS, Pan-STARRS, Virgo, Liverpool Telescope, BOOTES, LIGO Scientific, LOFAR, C2PU, MAXI), Astrophys. J. **826**, L13 (2016), arXiv:1602.08492 [astro-ph.HE].

[109] F. Foucart, M. B. Deaton, M. D. Duez, L. E. Kidder, I. MacDonald, C. D. Ott, H. P. Pfeiffer, M. A. Scheel, B. Szilagyi, and S. A. Teukolsky, Phys. Rev. D **87**, 084006 (2013), arXiv:1212.4810 [gr-qc].

[110] T. Hinderer *et al.*, Phys. Rev. Lett. **116**, 181101 (2016), arXiv:1602.00599 [gr-qc].